# Table of Contents – Chapter V

Page


1.4 Improved AUT Imaging and Defect Identification ..... 1

1.4.1 Information Extraction from Data File Format ..... 1

1.4.1.1 Data Retrieval ..... 1
1.4.1.2 Basics on Displaying Data ..... 2
1.4.1.2.1 1- and 2D Display of Data ..... 2
1.4.1.2.2 Special Type of 2D Display – S-Scans ..... 5
1.4.1.2.3 Noise-Removal Concept ..... 9
1.4.1.2.4 The Nature of Wedge Noise in AUT System ..... 10
1.4.1.2.5 Overview of Wedge Noise Removal Algorithm ..... 11
1.4.1.2.6 Implementation of the Wedge Noise Removal Algorithm ..... 14
1.4.1.2.7 Other Types of Noise Removal Algorithm ..... 15
1.4.1.2.8 3D Imaging Concepts ..... 15
1.4.1.2.9 Basic 3D Reconstruction of an Object ..... 16
1.4.1.2.10 2½D Display of Data (Scans with Physical Dimension of Parts in Mind) Thickness-Corrected B-Scans and Beyond ..... 19
1.4.1.2.11 Initial Development of 3D Imaging ..... 22
1.4.1.2.12 Individual Defect Extension through B-scans ..... 27

1.4.1.3 Conclusion ..... 29
1.4.1.4 References ..... 29

1.4.2 AUT Data Fusion and Improved Sizing and Analysis Techniques ..... 31

1.4.3 Establishing Improved Ultrasonic Test Sensitivity Levels ..... 42


## Tables


Table 1.4.1-1. Test Data (Note that this Coordinates are Sequentially Arranged) ..... 16

Table 1.4.1-2. Revised Test Data Array ..... 18


## Figures


Figure 1.4.1-1. Arrangement of Scan Data ..... 2

Figure 1.4.1-2. Typical Rectified A-Scan ..... 3

Figure 1.4.1-3. Basic Principle of C-Scan ..... 4

Figure 1.4.1-4. C-Scan Image ..... 4

Figure 1.4.1-5. Principle of B- and D-Scans ..... 6

# Table of Contents – Chapter V

Page


Figure 1.4.1-6. Typical B- and D-Scan Images ..... 7

Figure 1.4.1-7. Electronic Scanning and Data to be Displayed ..... 8

Figure 1.4.1-8. Typical S-Scan ..... 8

Figure 1.4.1-9. Noise Generated by the use of Wedges ..... 10

Figure 1.4.1-10. C-Scan Corresponding to the Wedge Noise ..... 12

Figure 1.4.1-11. Regions Where Wedge Noise Takes Place Also Contains Defects ..... 13

Figure 1.4.1-12. Screen Shot from Wedge Noise Removal Program ..... 14

Figure 1.4.1-13. Simplified Box for 3D Reconstruction ..... 17

Figure 1.4.1-14. Display of Test Data from Table 1.4.1-1 ..... 17

Figure 1.4.1-15. Successful Representation of 3D Box ..... 18

Figure 1.4.1-16. Angle-Corrected B-Scan of a Machined Slot ..... 20

Figure 1.4.1-17. Fold-Back B-Scan Based on Angle of Projection on PA UT Beam ..... 21

Figure 1.4.1-18. Threshold-Processed Data ..... 24

Figure 1.4.1-19. Linked and Grouped Defect Data ..... 25

Figure 1.4.1-20 3D Wire Frame of Folded Data Boundary ..... 26

Figure 1.4.1-21. An Exemplary 3D Representation of Defect Map ..... 28

Figure 1.4.2-1. Example of UT Data Display Techniques ..... 33

Figure 1.4.2-2. Proposed Time-Based Sizing of a Crack Using PA UT ..... 34

Figure 1.4.2-3. Fused D-Scan Views of 61.0-cm-Diameter Girth Weld ..... 34

Figure 1.4.2-4. Multi-Angle D-Scan View of a Through-Wall Fatigue Crack in 11.7-mm (0.46-in.)-Thick Pipe Wall ..... 35

Figure 1.4.2-5. Fused D-Scan Views for US Scan ..... 36

Figure 1.4.2-6. Fused D-Scan Views for DS Scan ..... 36

Figure 1.4.2-7. Polar View for DS Scan ..... 37

Figure 1.4.2-8. Zoomed Polar View for DS Scan ..... 37

Figure 1.4.2-9. Multi-Angle D-Scan View for US Scan ..... 38

# Table of Contents – Chapter V

Page


Figure 1.4.2-10. Multi-Angle D-Scan View for DS Scan ..... 38

Figure 1.4.2-11. Multi-Angle D-Scan View for US Scan with Second Leg Folded up on First Leg..... 39

Figure 1.4.2-12. Multi-Angle D-Scan View for DS Scan with Second Leg Folded up on First Leg..... 39

Figure 1.4.2-13. Multi-Angle D-Scan View with US and DS Data Fused and Second Leg Folded up on First Leg..... 39

Figure 1.4.2-14. A- and S-Scan Views of Flaws on the US and DS Weld Bevels ..... 40

Figure 1.4.3-1. EWI-1 Calibration Reference Sample..... 43

Figure 1.4.3-2. Comparison of the Reflection from a 1.2-mm SDH Compared to 10-mm-Long Notches with a Range of Through-Wall Heights..... 44

Figure 1.4.3-3. Typical Reflected Signal from the Face of a 3-mm FBH used for LCP Zone in Calibration Sample EWI-1 ..... 45

Figure 1.4.3-4. EWI-2 OD and ID Notch Calibration Sample..... 47

Figure 1.4.3-5. 40-Degree Beam Angle Intersecting Radial ..... 48

Figure 1.4.3-6. PA AUT Scan of ID Notches Oriented Parallel to the Longitudinal Pipe Axis..... 48

Figure 1.4.3-7. PA AUT Scan of OD Notches Oriented Parallel to the Longitudinal Pipe Axis..... 49

Figure 1.4.3-8. PA AUT Scan of ID Notches Oriented Perpendicular to the Longitudinal Pipe Axis..... 49

Figure 1.4.3-9. PA AUT Scan of OD Notches Oriented Perpendicular to the Longitudinal Pipe Axis..... 50

Figure 1.4.3-10. Tandem Techniques for Detection of Weld Bevel Fusion Flaws..... 51

## 1.4 Improved AUT Imaging and Defect Identification

In this section, the effort on the development of improved AUT imaging program is described. It is the hope of the developer that this introduction can provide some insight as to the basic principles of the data file retrieval and display to the user of this program to gain understanding of the working principles of the process.

### 1.4.1 Information Extraction from Data File Format

The most fundamental aspect of an ultrasonic data file is, as the name implies, the individual UT waveform data (e.g., A-scans). In the simplest form of the data file, the file itself will contain only scan data arranged in a format that is recognizable to all programs. Due to the fact that there are a variety of UT system manufacturers; however, it may not be possible to decode a given data file if no prior understanding of how the data itself is arranged. In addition, there might be need for the data files to contain additional information such as the distance to the reference point, scan intervals, increments, as well as hardware settings so as to successfully decode the data contained in a file, and represent the data in a meaningful fashion.

In the following section, the methodology of decoding one of the proprietary file formats will be discussed as an example of how information can be stored into a data file for archival purposes.

#### 1.4.1.1 Data Retrieval

Once the data items have been decoded, the relevant portion (or the actual data content) can then be retrieved through the known pointer(s) acquired through various locations embedded in the data items. Additionally, all other relevant parameters (such as speed of sound in the material, transducer angle, pulser/receiver frequency settings) can also be retrieved to arrange the data to easy-to-understand presentation format, and can be displayed in a graphical format such that users can easily understand the locations and the size of the flaw.

As mentioned in the introduction, the data in its purest form contains nothing else but ultrasonic waveform acquired by the receiver and analog-to-digital converter (A/D cards.) In addition, individual data points consists of 1 byte in the data file space (unsigned 8-bit integer). On the other hand, if an area was inspected as opposed to a single point on the part surface, the data will have to be stored and retrieved in an orderly fashion to truly represent the physical correspondence of individual waveforms (Figure 1.4.1-1). Also, as a consequence, the amount of data increase with respect to the number of surface points the inspection is to take place. As seen in Figure 1.4.1-1, the top surface of the cube shows the locations at which an ultrasonic waveform are acquired (represented by rows and columns), and samples represent the

ultrasonic waveform data (in array format) for that particular location. It is, therefore, conceivable that the scanning pattern plays an important role in reconstructing the data, as well as the order of scanning itself.

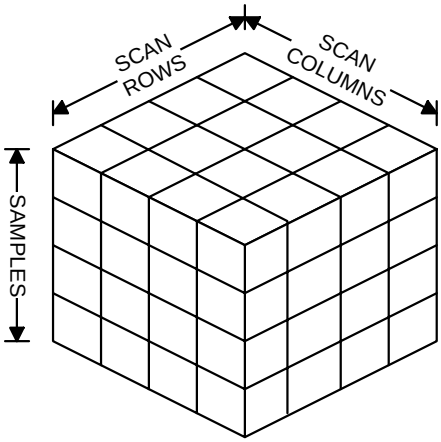


**Figure 1.4.1-1. Arrangement of Scan Data**

Furthermore, due to the fact that not all ultrasonic measurements use straight beam longitudinal wave (L-wave), it is likely that the data arrays will need to be corrected for the transmitting angle to account for the actual internal feature locations. In addition, if the ultrasonic system used in acquiring data is capable of electronic scanning (i.e., PA system), it is also likely that there will be more than one groups of data contained in the data file. These additional factors complicate the data representation significantly, and need to be addressed separately to ensure the correctness in representing the data. These aspects will be discussed in more detail in the following section.

### 1.4.1.2 Basics on Displaying Data

#### 1.4.1.2.1 1- and 2D Display of Data

As stated in the previous section, once the data arrays are acquired and arranged properly, the program can then present the data in the format that best describe the physical attributes, and conforms to established standards. Typical means of representation include A-, B-, C-, and D-scans, and in the case of PA systems, a sectorial scan (S-scan). A-scans are the most commonly used means of displaying an ultrasonic waveform data type, as it shows the amplitude information for the whole duration of the waveform data, with the abscissa represented either in data point counts, time, or in physical distance. Figure 1.4.1-2 shows a typical rectified A-scan.

C-scans, on the other hand, display an aerial (top) view of the full area under inspection at a certain depth from the part surface. Since the data file was such arranged that all the A-scan data arrays were aligned based on the order (in rows and columns) as they were acquired, a C-scan image at a certain depth would be similar to taking a cross section of the aggregate A-scan cube horizontally at a specified distance parallel to the part surface, as indicated in Figure 1.4.1-3. The benefit of using a C-scan image is that the features along the same depth can easily be visualized, as seen in Figure 1.4.1-4.

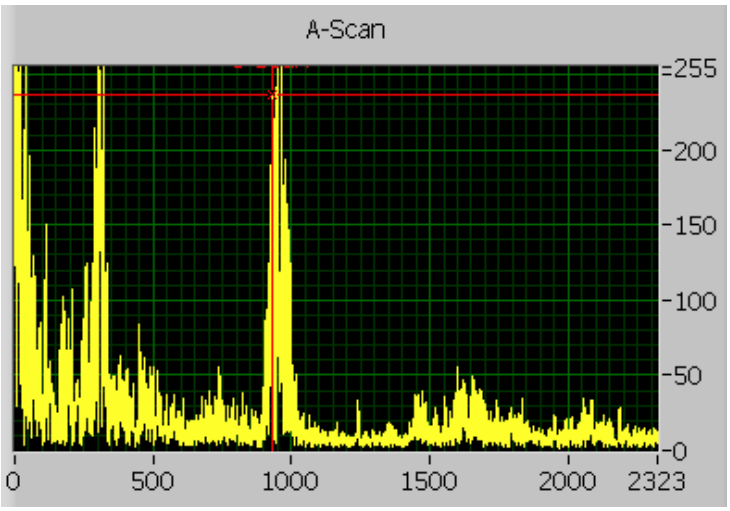


**Figure 1.4.1-2.** **Typical Rectified A-Scan** (Note that the Abscissa is denoted by the number of data points.)

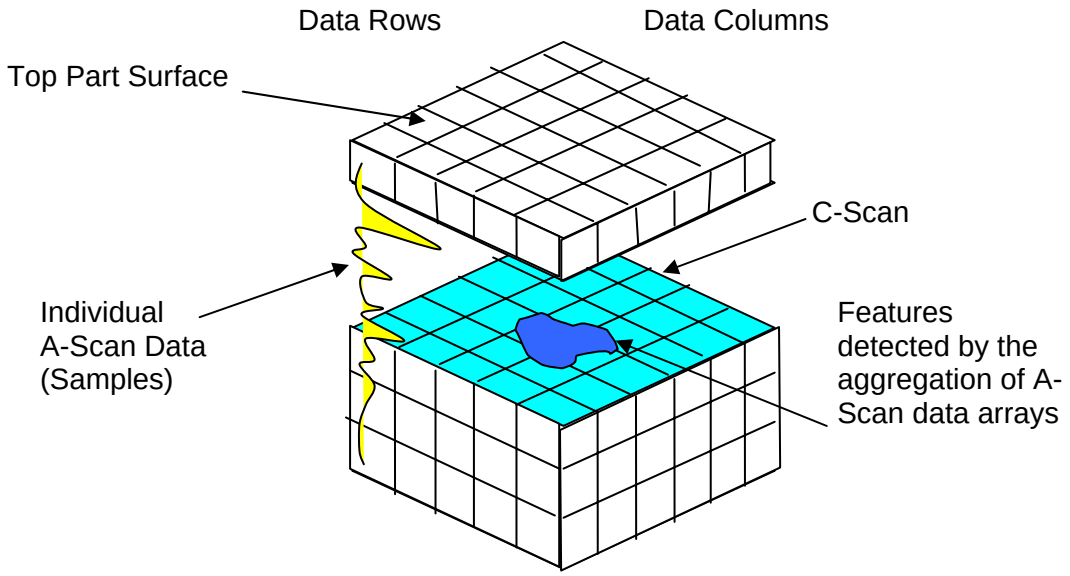


**Figure 1.4.1-3. Basic Principle of C-Scan**

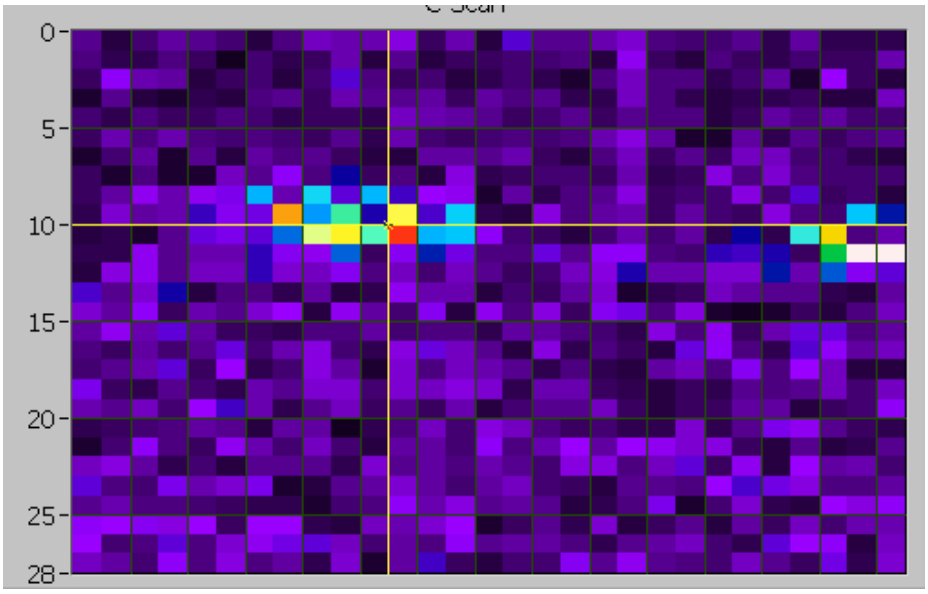


**Figure 1.4.1-4. C-Scan Image**

By the same token, both B- and D-scans are similar in concept to that of C-scans. There is a major difference, however, between the C- and B- (or D-) scans in that the orientation of cross sectioning is different between that of B-, C-, and D-scans. Depicted in Figure 1.4.1-4, C-scans are cross sectioned parallel to that of the part surface, yet B- and D- scans are cross sectioned perpendicular to the part surface. In addition, between the B- and D-scans, the cross sections are 90-degrees apart, as shown in Figures 1.4.1-5 and 1.4.1-6.

#### 1.4.1.2.2 Special Type of 2D Display – S-Scans (Sectorial Scans)

The S-scans are a special type of 2D display of data in the sense that it is only available in the PA system under which the electronic scanning scheme is used. The direct result of using electronic scanning scheme is that under the same surface location at which the ultrasonic wave is fired and received, a triangular fan of 2D area can be covered, and a cross section can thus be created based on the data acquired. As a consequence, the S-scan map can provide with the inspectors with more information within the same spot of inspection as the data is acquired from within the same location to cover an area that the inspector is interested in. As shown in Figures 1.4.1-7 and 1.4.1-8, an area is scanned and data regarding that area is acquired and displayed.

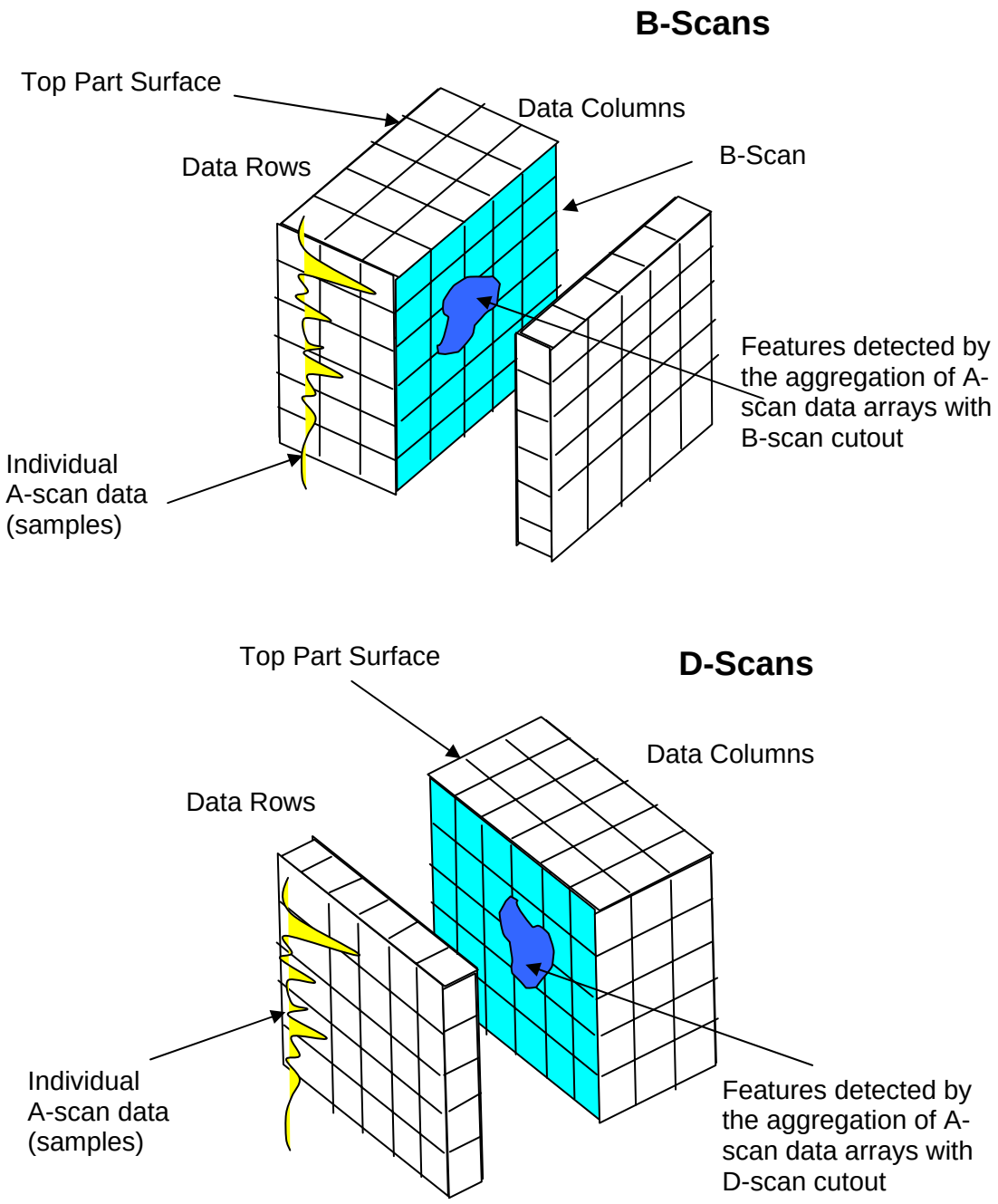


**Figure 1.4.1-5. Principle of B- and D-Scans**

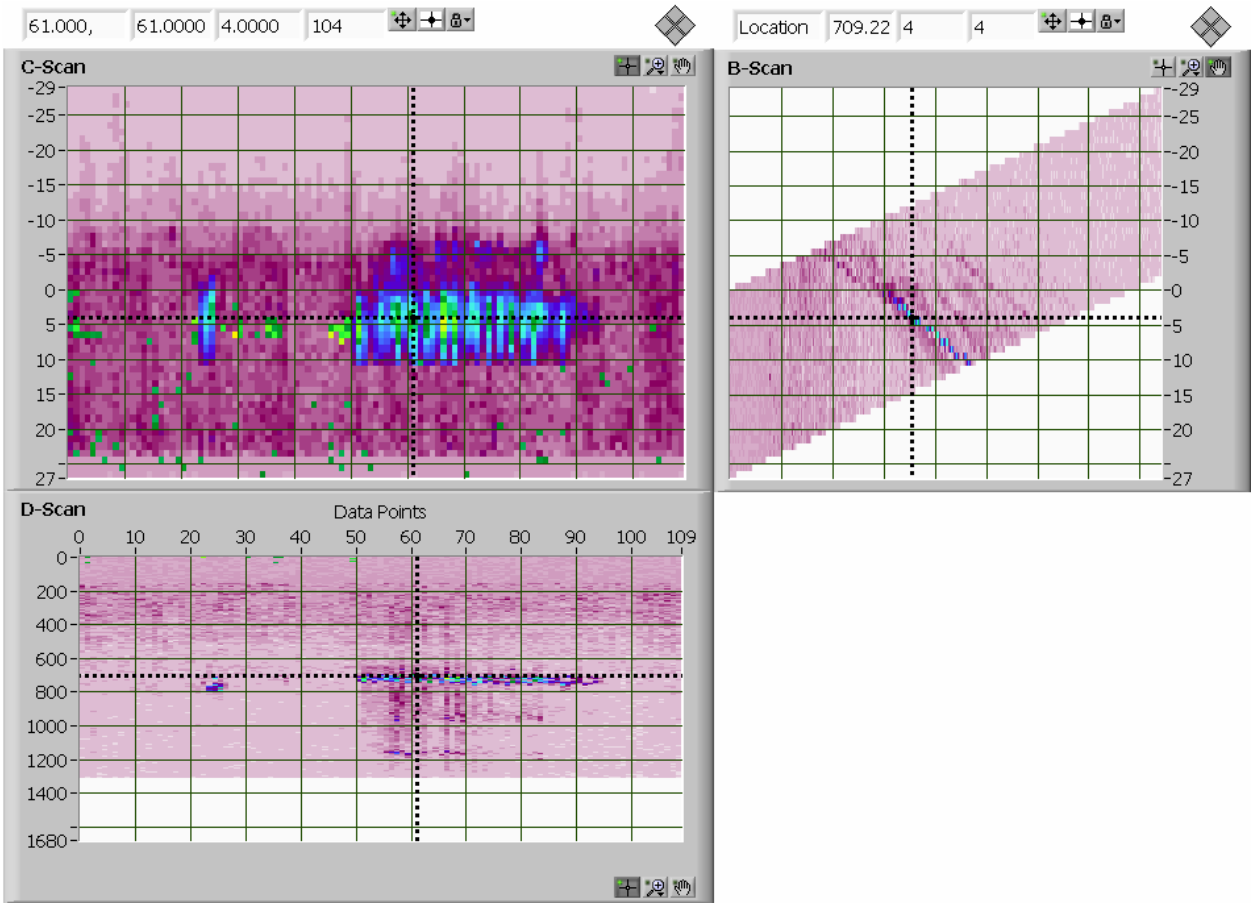


**Figure 1.4.1-6. Typical B- and D-Scan Images (with respect to C-Scans)**

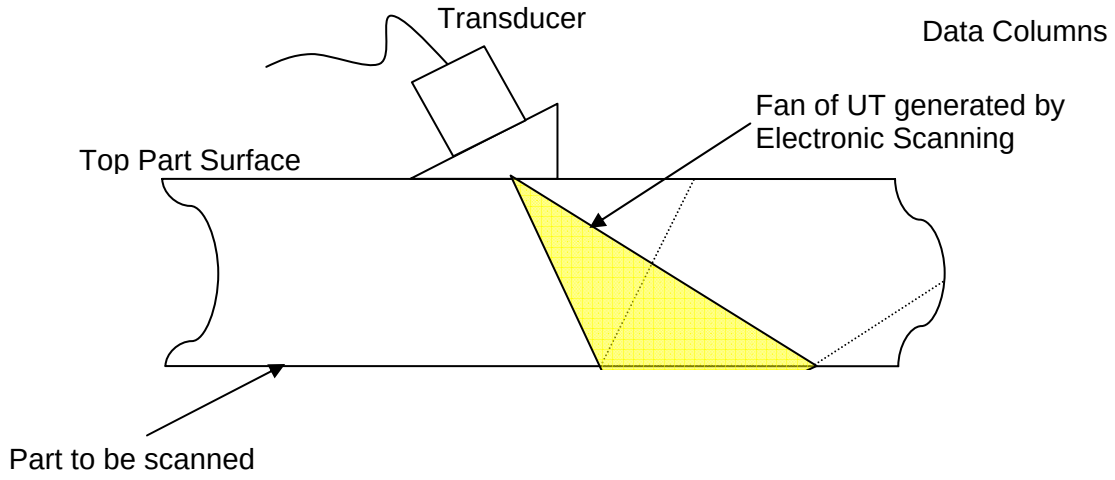


**Figure 1.4.1-7. Electronic Scanning and Data to be Displayed**

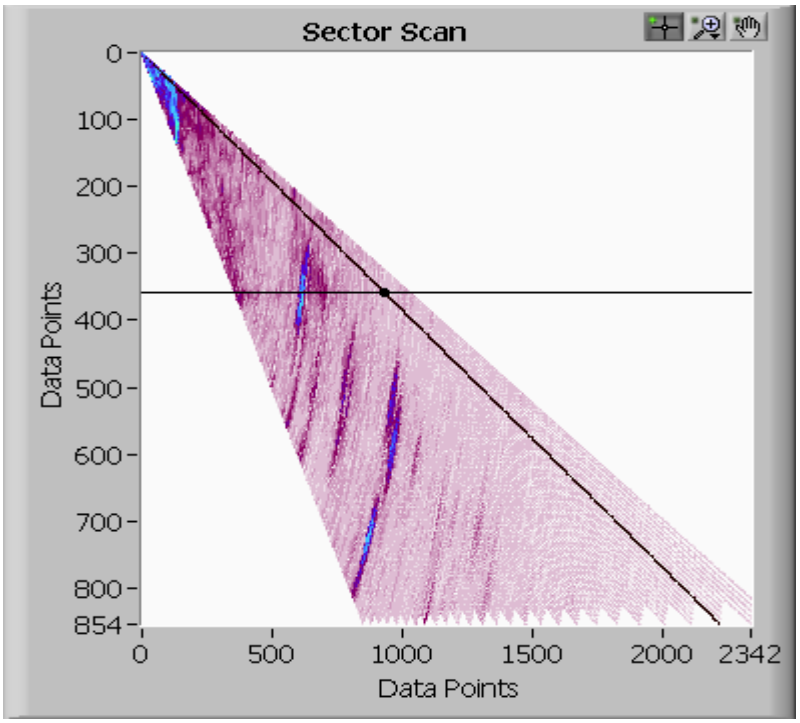


**Figure 1.4.1-8. Typical S-Scan**

There are advantages as well as disadvantages for using the electronic scanning/S-scans. The advantages include the following:

- Advantages
  - User can gain volumetric information (2D information) regarding a particular area of interest without even moving the transducer, as the firing and receiving angles of a transducer array are steered electronically.
  - A vast amount of data can be generated without a significant amount of motion. For example, to create a 3D map of a certain area, only 1D motion is required (as the other two dimensions can be controlled by electronic scanning).
  - It is possible for inspector to acquire data from hard-to-reach locations (for example, locations where access of physical transducers is impossible.) Data can easily be re-constructed for determination.
- Disadvantages:
  - A vast amount of data is available, which requires more powerful equipment (computer processing power, A/D card, storage, etc.)
  - Displaying the data becomes a non-trivial issue. Specifically, when a 2D surface is scanned, it is likely that some portion of data will overlap one another, which creates data redundancy. Data redundancy will further increase the burden in data processing.

To address the disadvantage in terms of data manipulation as well as representation, special algorithms will have to be adopted. The basic concept of the algorithms will be depicted in the sections that follows (Sections 1.4.1.2.3 to 1.4.1.2.6).

#### 1.4.1.2.3 Noise-Removal Concept

As is the case in any measurement systems, NDT equipment that uses ultrasonic (or ultrasonic PA) techniques are bound to be susceptible by noise. In this section, a simple algorithm that addresses to the issue of one of the most prominent type of noise will be illustrated, and the discussion on the implementation of the algorithm will also be given.

#### 1.4.1.2.4 The Nature of Wedge Noise in AUT System

As stated above, the UT measurements are susceptible to noise. Specifically, when it comes to a PA system, the noise generated by the use of wedges is prominent (as shown in Figure 1.4.1-9), and can easily be identified as noise. The characteristics of wedge noise are that the noise will be universal cross all A-scans at approximately the same location, e.g., the effect of wedge noise will be concentrated at a certain depth for all the A-scans (as determined by the inspectors). When the A-scans are displayed into either B- or D-scans, the rationale in determining the noise components as wedge is by observing the B- (or D-) scans. If a band of signal runs across the full width of the scans, it is likely that the whole band if signals consists of wedge noise.

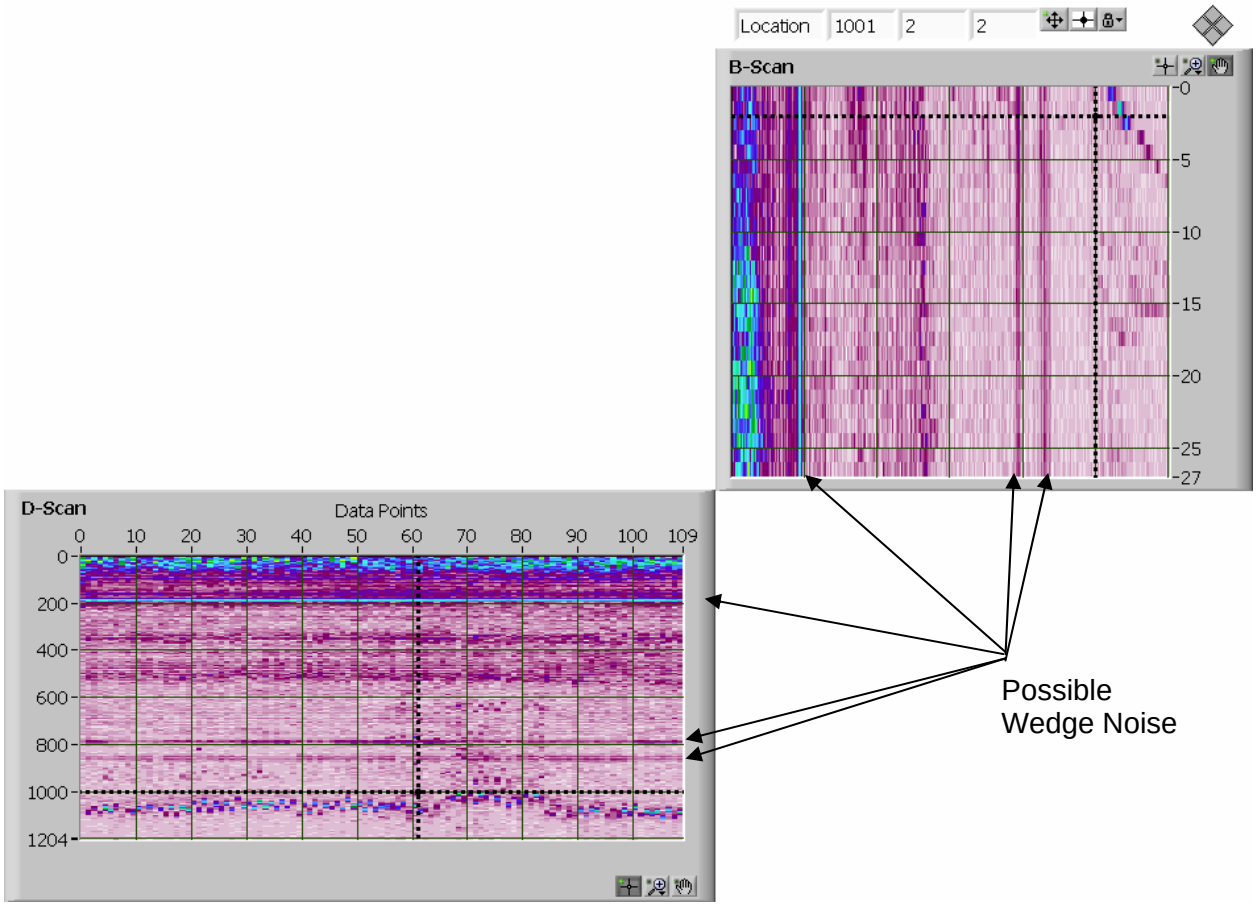


**Figure 1.4.1-9. Noise Generated by the use of Wedges**

Unfortunately, it is unlikely that an inspector can remove the noise easily unless wedges are not used. As a consequence, the inspectors will have to determine the existence of a defect from data that contains wedge noise. In the following section, an algorithm that will remove the wedge noise is proposed, and the implementation of the algorithm will also be described.

#### 1.4.1.2.5 Overview of Wedge Noise Removal Algorithm

As stated in the previous section, the occurrence of wedge noise is unavoidable. However, since the data was already recorded, it is possible to process the data and remove the noise signals at locations where the inspectors are certain that signals are noise in nature. Thus, it is proposed that an algorithm be developed that can perform a localized but universal noise on all of the A-scans, and replace the signals within the specified region with a known, non-noisy data value across all the A-scans. A detailed description is as follows.

When a data file is displayed in terms of all the A-, B-, C-, and D-scans, it is likely that an inspector can determine where the locations are that the wedge occurred (as shown in Figure 1.4.1-9 where the light-blue band and dark purple bands occurred). By the same token, if the bands of color appear by observing the B- and D- scans, it is likely that the corresponding C-scans at these locations will consist of mostly noisy signals, as depicted in Figure 1.4.1-10. Thus, the complete C-scan at the location should be replaced by normal data values.

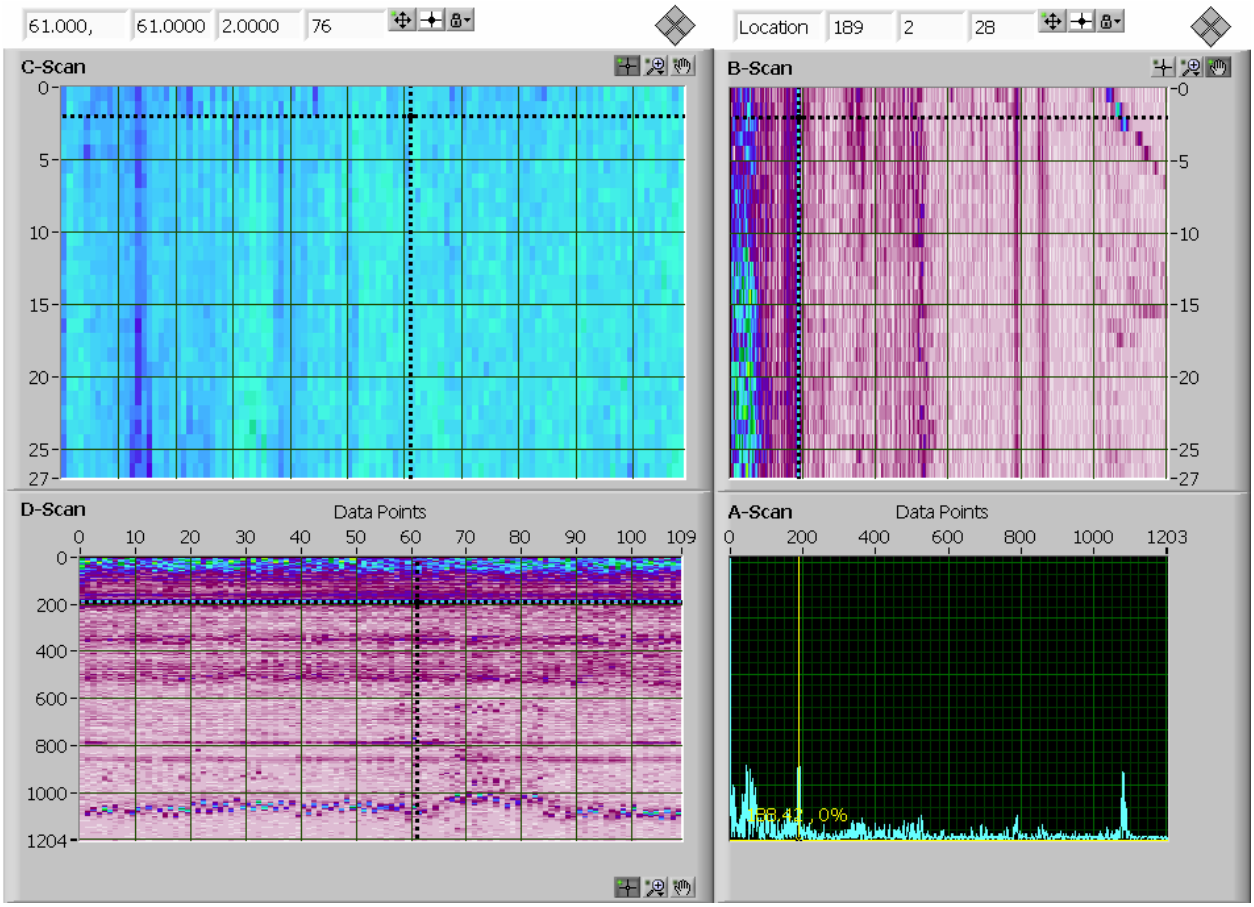


**Figure 1.4.1-10.** **C-Scan Corresponding to the Wedge Noise** (A-scan cursor indicates the location of C-scan.)

In other words, it is assumed that the wedge noise will compose the majority of the C-scan when it does occur, and can be determined with a percentage number at which the C-scans are filled with the data values of a certain range.

As another example, however, it is possible that there are actual features or defects in the region where the wedge noise exists, as shown in Figure 1.4.1-11. When this is the case, it is necessary to preserve the actual features while removing all the noise content. Thus, a high-value threshold feature will be necessary to retain the signals that are over this threshold. In addition, the application of filters may not be all-inclusive, i.e., sometimes it may require more than one iteration of filters being applied before all the wedge noise can be removed.

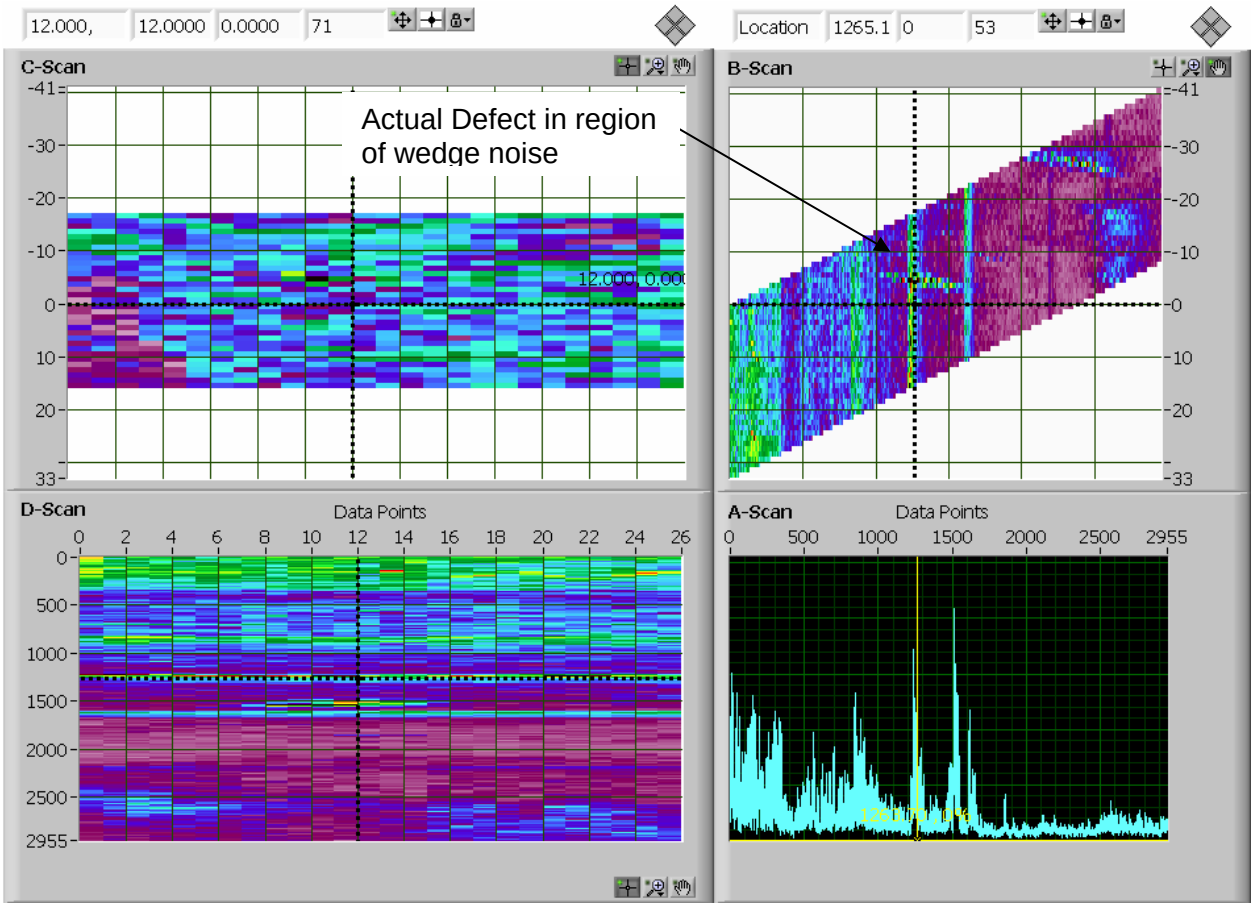


**Figure 1.4.1-11. Regions Where Wedge Noise Takes Place Also Contains Defects**

To summarize, a successful algorithm for wedge noise removal will have to contain the following features:

- Low and high thresholds for noise removal. Only the signals that fall within the low and high thresholds will be filtered, and these thresholds should be adjustable based on inspector inputs.
- User-definable regions for filter application, as well as user-defined percentage for C-scans that fall under the filter thresholds before the application can take place.
- Multiple iterations of filtering should be available.
- User-defined replacement values for regions to be filtered.

#### 1.4.1.2.6 Implementation of the Wedge Noise Removal Algorithm

As shown in Figure 1.4.1-12, the screen shot of a typical wedge noise removal program can contain the following displays:

- Original B-scan
- Filter Screens 1, 2, and 3
- Filter progress indicators
- Amplitude color scale, as well as filter threshold sliders for individual filters (represented by F-1, -2, and -3)
- Percentage of data in C-scan within thresholds
- Replacement data value for individual filters.

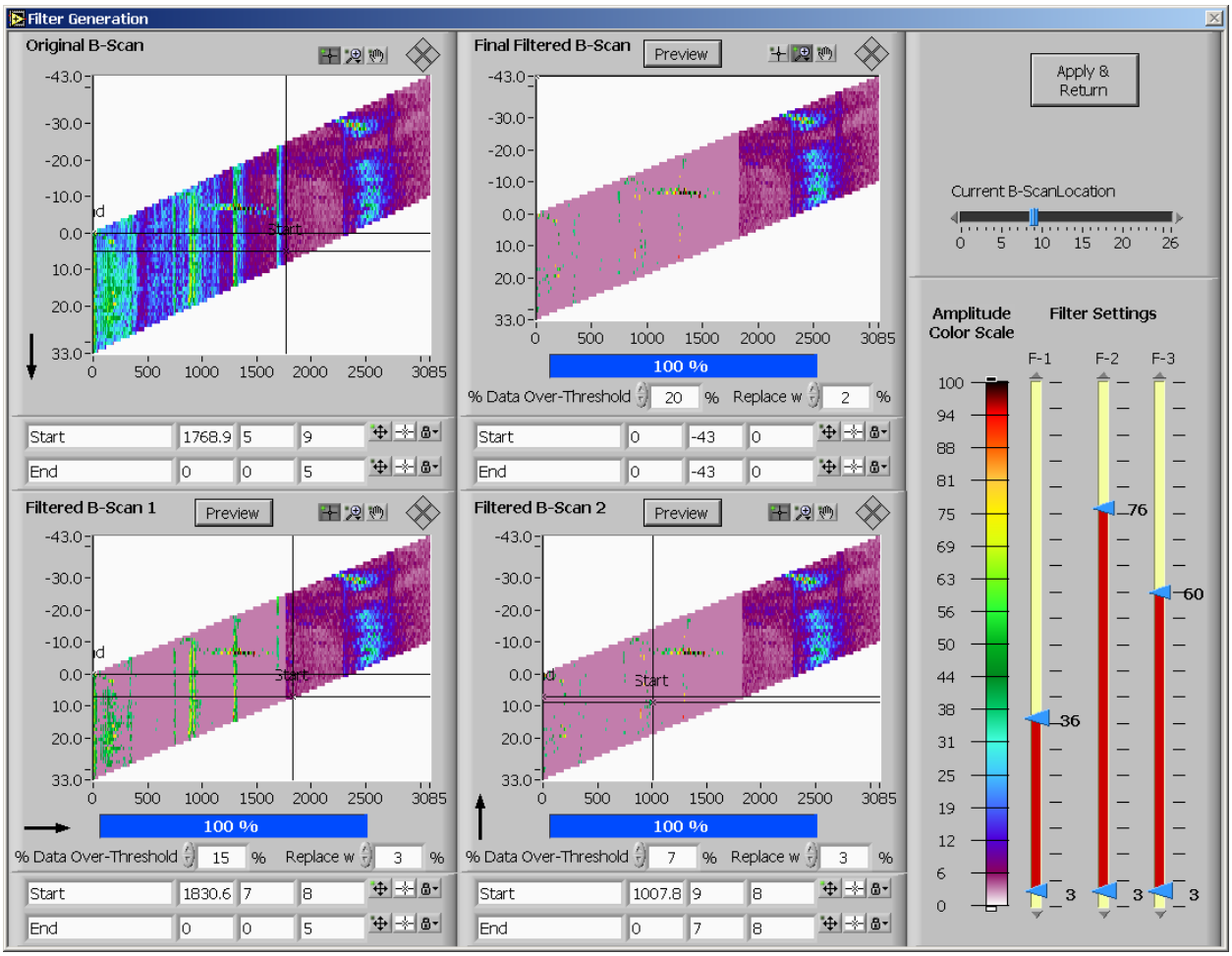


**Figure 1.4.1-12. Screen Shot from Wedge Noise Removal Program**

The top left image in the screen shot represents the original B-scan from the data file. The inspector will follow the procedures to remove the wedge noise as follows:

- The inspector determines the region at which the noise removal algorithm should be applied by moving the start and end cursors to the corresponding location (in the original B-scan) for F-1.

- Move the F-1 threshold sliders next to the color scale (F-1), only the data that fall within the red portion will be filtered (the data values outside the thresholds are unaffected).

- Define the percentage at which the C-scans data points are within the thresholds.

- Enter the replacement data values.

- Press Preview button to see the result of F-1 in the filtered B-scan 1 window.

The same procedures can be repeated for up to three times, until the user is satisfied with the filter results. As long as the program is executing, the user can run as many scenarios of desired filter schemes as needed without actually apply these filters. In addition, the user can also scroll through all available B-scans to see if some defects are inadvertently removed, and the filter settings need to be re-configured to preserve these features.

#### 1.4.1.2.7 Other Types of Noise Removal Algorithm

Other types of noise removal algorithms include (but not limited to) localized averaging filters that focus on only a user-defined region (in terms of width and height on a particular B-scan), or filters that use the matrix-weighted average of nearby data values (use the nearby data values in the surrounding matrix (3 × 3, 5 × 5, 7 × 7, 9 × 9, or more) to perform weighted average to attain filtering). In addition, the same types of filtering can also be used with respect to C- or D-scans.

#### 1.4.1.2.8 3D Imaging Concepts

In this section, the basics of 3D imaging will be provided as a reference. Some reference material can be found in the following reference.[(1.4.1-1 through 1.4.1-5)]

#### 1.4.1.2.9 Basic 3D Reconstruction of an Object (Specific to Programming Environment)

In order to present an object in a 3D space (for defect representation purposes), it is necessary to understand the basics of computer graphics used in the software development environment. The following descriptions provide a brief, concise look at how an exemplary rectangular cube is re-constructed.

##### 1.4.1.2.9.1 Test Data Generation and Resultant Imagery of 3D Representation

The most simplified version of a 3D object can be illustrated using the concept of a box. Figure 1.4.1-13 depicts a box that is to be represented in 3D. The rationale behind this much simplified object is to deduce the methodology from which any polygonal objects with multiple facets on the object can be accurately depicted using the same method for successful reconstruction into a 3D image.

**Table 1.4.1-1. Test Data (Note that this Coordinates are Sequentially Arranged)**

| X (Row) Array | | Y (Column) Array | | Z (Depth) Array | |
|---|---|---|---|---|---|
| 0 | 0 | 0 | 5 | 1 | 1 |
| 10 | 10 | 0 | 5 | 1 | 1 |
| 0 | 0 | 0 | 5 | 0 | 0 |
| 10 | 10 | 0 | 5 | 0 | 0 |

The first set of test data was generated in order to provide all necessary point coordinates to provide with end-point information (e.g., all apexes were described in terms of three 2D arrays for the purposes of denoting the spatial relations between data points in 3D with X, Y, and Z coordinates). It was assumed that with this information available, the programming environment should be able to re-construct a box-type image that represents the constructs that represent a rectangular cube.

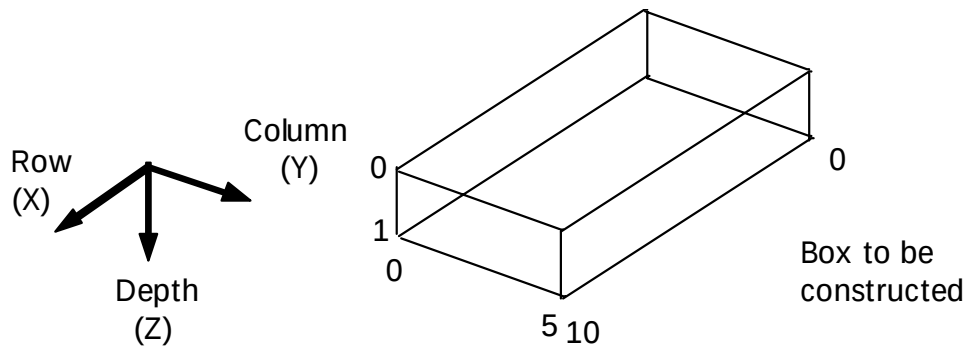


**Figure 1.4.1-13.** **Simplified Box for 3D Reconstruction** (The Cartesian coordinates are shown on the left.)

After the test data arrays have been input into the graphic generator and plotted into a 3D image the following image was generated (as shown in Figure 1.4.1-14). Note that the original test data only displayed three facets of the rectangular cube: bottom, top, and a slope plane that was not part of the desired box surfaces. The reason being that the computer graphic generator treats the consecutive data points as continuous plane coordinates and reconstruct them sequentially in order to achieve the continuity of the planar information. As a consequence the data arrangement (and reduction for that matter) needs to be tailored to conform to the final shapes of the objects to be plotted.

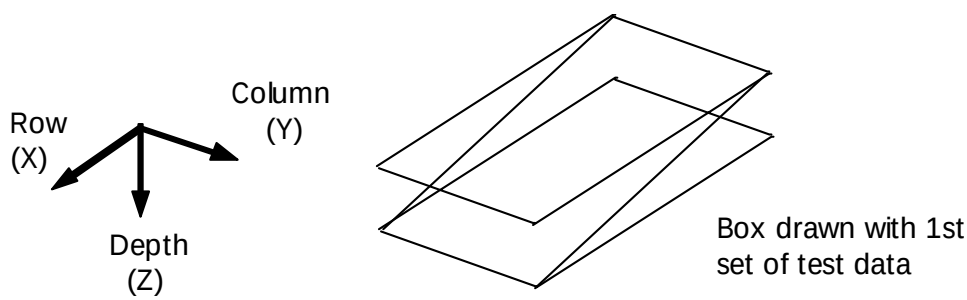


**Figure 1.4.1-14.** **Display of Test Data from Table 1.4.1-1**

A new set of data arrays were subsequently generated to attempt to plot the desired box in 3D space. The data arrays are presented in Table 1.4.1-2.

**Table 1.4.1-2. Revised Test Data Array**

| X (Row) Array | | Y (Column) Array | | Z (Depth) Array | |
|---|---|---|---|---|---|
| 0 | 0 | 0 | 5 | 1 | 1 |
| 10 | 10 | 0 | 5 | 1 | 1 |
| 10 | 10 | 0 | 5 | 0 | 0 |
| 0 | 0 | 0 | 5 | 0 | 0 |
| 0 | 0 | 0 | 5 | 1 | 1 |
| 0 | 0 | 5 | 5 | 1 | 0 |
| 10 | 10 | 5 | 5 | 1 | 0 |
| 10 | 10 | 0 | 0 | 1 | 0 |
| 0 | 0 | 0 | 0 | 1 | 0 |

The 3D plot generated by this set of data arrays is shown in Figure 1.4.1-15.

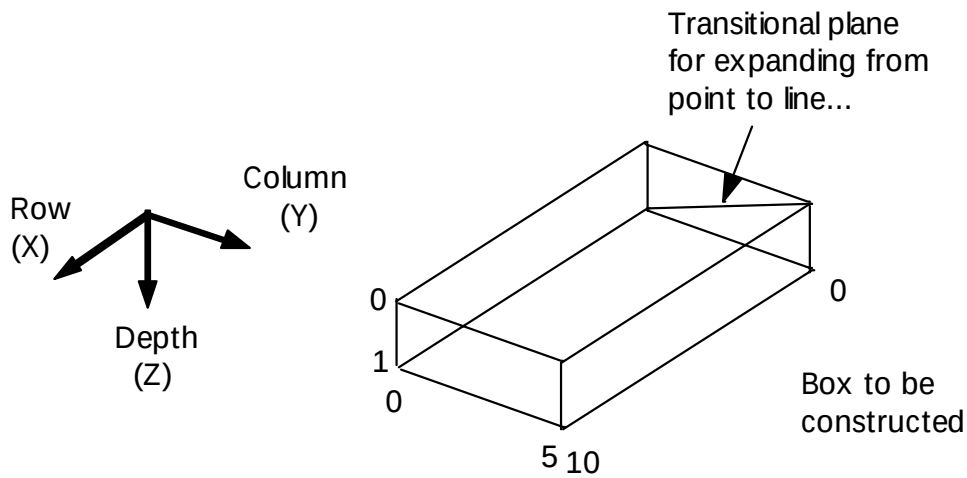


**Figure 1.4.1-15. Successful Representation of 3D Box**

It is demonstrated that in order to present ALL facets of a cube, ALL planes have to be described numerically with possibly the following rules:

- All facets have to have end points numerically input into arrays.
- It is preferred that the plane descriptions be followed (e.g., the end points with at least one end point attached from the previously described plane). In addition, to prevent the transitional plane(s) from being generated, it is recommended that the mechanisms that will generate the arrays reduce the line into a point, and expand point into a new line for the next plane, and so on. (This item will be explained in more detail once the actual codes are generated.)

- Cases exist that end points need to be duplicated to transition from one plane to another. In other words, it may be necessary to duplicate some portion of the end point coordinates to realize the reconstruction without relational lines generated erroneously.

#### 1.4.1.2.10 2½D Display of Data (Scans with Physical Dimension of Parts in Mind) Thickness-Corrected B-Scans and Beyond

To be able to represent a physical defect in 3D space, it is necessary to know the physical boundary at which the ultrasonic wave progresses (geometrical constraint or boundary), as well as the dispersion of the UT wave propagation itself. That is, it is not possible to re-produce the defect in 3D without knowing the part dimensions, and it is also essential to understand the physics of UT wave propagation in material in order to represent the defects in the correct locations for a given part.

For simplicity, the treatment of the defect representation in 2½D will address only with the underlying geometry without introducing the UT wave propagation physics (such as beam spread in a PA UT wave propagation). In addition, some UT signal features that are useful in determining the defects for inspectors (for example, corners, tips signals, etc.) will not be considered into the 3D representation of the data until later date, as it involved more complex data manipulation schemes than the scope of the project.

From the rationale above, consider a flat part with the thickness of 1 in. (25.4 mm) and the width that is much wider than that of the scanning area of a motion device. If a defect was manufactured on either the top or bottom surface, and a PA probe was used to detect the machined slot which is about half of the thickness of the material (13 mm) then the resulting scans may look like the following figure [Figure 1.4.1-16 (with filtering to remove wedge noise)].

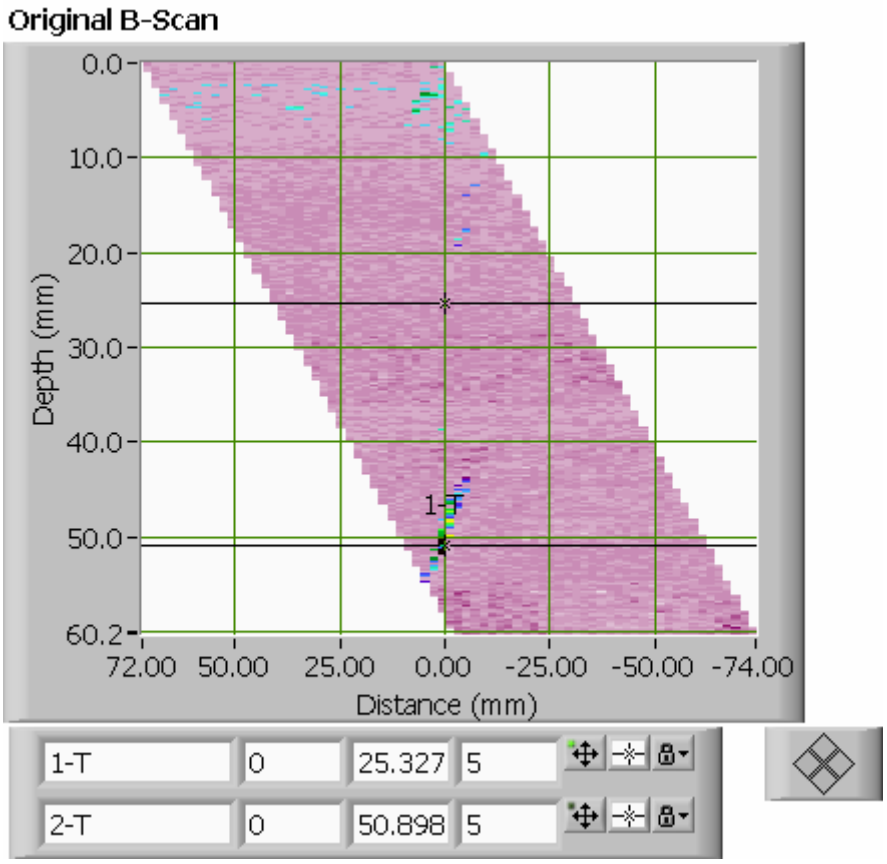


**Figure 1.4.1-16. Angle-Corrected B-Scan of a Machined Slot**

As can be seen, the thickness indicators showed that the data acquired includes UT wave propagated through more than twice of the material thicknesses (as indicated by 1- and 2T). Note that the data is clearly beyond the physical material thickness, thus some manipulation in the data is needed in order to represent the defect geometrically.

The simplest form of data manipulation is to “fold” the data according to the angle at which the UT beams are projected, e.g., to overlap the data back to where the data points are supposed to be located physically according to the focal laws that were used to project the UT beams into the material. The result can be seen in Figure 1.4.1-17.

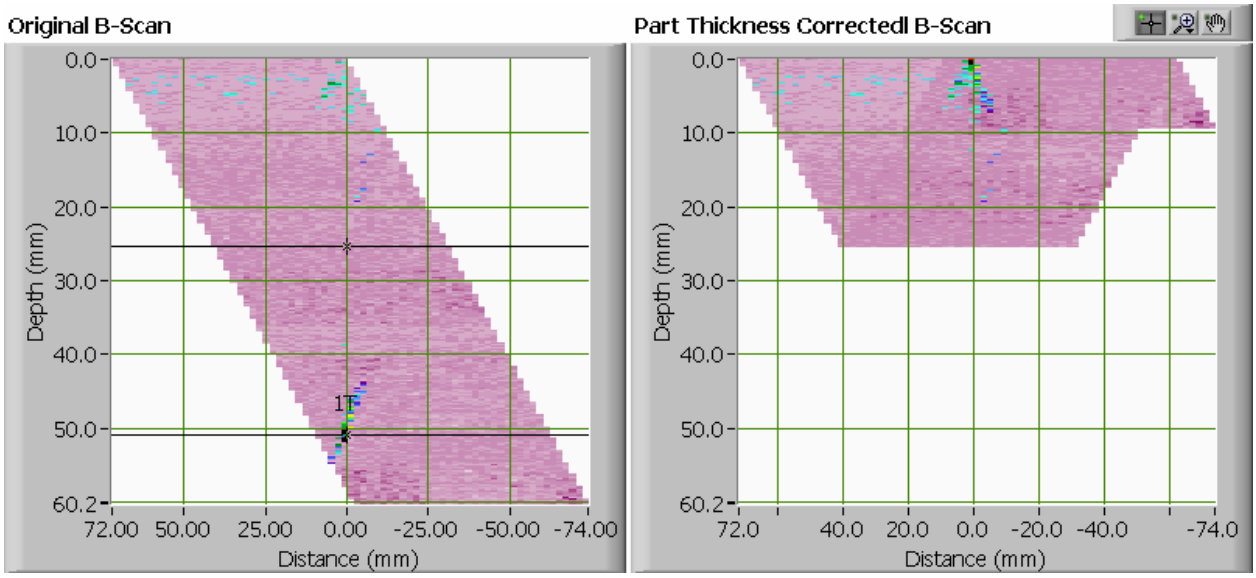


**Figure 1.4.1-17. Fold-Back B-Scan Based on Angle of Projection on PA UT Beam**

As can be seen, in the original angle-corrected B-scan, the defect appears to be in the bottom half of the scan, but in reality the defect should have been on the top surface. The “fold back” data manipulation scheme thus overlaps the data back to their “original” physical locations to re-construct the defect map shown in the right of the figure. If all of the B-scans contained in a file go through the same folding procedure, a line of defect will form at the location of approximately 0 mm in distance (starting position for scanning), and approximately 10 mm in depth (depending upon filtering results.) The aggregate of all the fold-back B-scans will thus become the 2½D display of the defect data, as individual slice of B-scans contain 2D of defect data, thus the slices of B-scans constitute the 2½D data groups where all the defects will be contained within all the B-scans.

One important thing to note in the data manipulation is that care has to be taken to ensure all of the data represented were presented in a real-world coordinate system, e.g., in representing the data, it is necessary to acquire geometry information not only for the A-scan data points (physical distance between data points acquired), but also the angle at which the PA UT beams were projected and acquired, as all of these geometric information play important roles in the data manipulation and orientation for the representation of defects in 2½D. In addition, the assumption of a flat part will have to be carefully examined as this assumption governs the validity of data arrangement such that defects can be represented correctly in their respective locations.

After the representation of 2½D data for one B-scan, one can infer that a full defect map can easily be generated to provide the basis of generation of a 3D defect map. Although this

inference is considered true for the most part, additional data processing is still required to generate necessary information for the true 3D defect representation. In the following sections, some of the basics will be addressed to provide a starting point for the successful representation of 3D defects.

#### 1.4.1.2.11 Initial Development of 3D Imaging

The initial concept of the 3D representation of defects originated back to the previous section: 2½D data representation by data fold-back. As seen in Figure 1.4.1-15, the data were folded back to represent approximately 2 and 1/3 times ("legs") of the material thickness (in angle-corrected format). After all the available B-scans go through the initial data fold-back, a series of 2D data with various amplitudes can be generated. Individually, each B-scan represents a slice of what the defects will appear for that particular distance index. However, it would be difficult for the software to categorize which part of the data on the scan belongs to which defects just by judging the amplitudes and locations alone, thus additional algorithms will need to be developed to try to size and categorize defects into groups.

The following provides a series of simplified version of algorithms for categorizing of the defects in preparation of 3D defect representation:

- Thresholding
- Linking and grouping
- Numbering of defects on single B-scan
- Boundary finding for folded data
- Continuation of defects in groups
- Individual defect extension through B-scans (grouping of defects through B-scans)
- Boundary generation for individual defect
- Defect surface generation (iteration)
- Overlaying of generated defect groups into bounded, folded data frame
- Defect generation and plotting.

A brief description is provided as follows:

- **Thresholding**

    - To determine whether or not a data point belongs to a defect or not depending upon the amplitude at which the data represents. A simple thresholding technique can help with the determination of data grouping. A threshold should be set up manually for the user to verify whether or not a point actually belongs to defect, or just a solid metal, and then the threshold can be applied throughout the B-scan to differentiate the defect data from metal data. An example continuing from previous section can be seen in Figure 1.4.1-18. Note that in the figure the thresholding helped decides whether a data point is valid for defect, or just regular metal data based on the amplitude. The outcome of the thresholding to then go through the data processing that follows.

- **Linking and Grouping**

    - The next step is to link and group the data from thresholding to create a more life-like defect. As can be seen from Figure 1.4.1-18, the major defect seen in the figure will be at distance 0 mm, with a fork-out shape, which is not a true representation of actual defect (machined slot). Additional algorithm is then used to try to bridge the defect forks into one meaningful defect, as well as filling out the voids that may be embedded into the defect lines. The results of the algorithm can be seen in Figure 1.4.1-19.

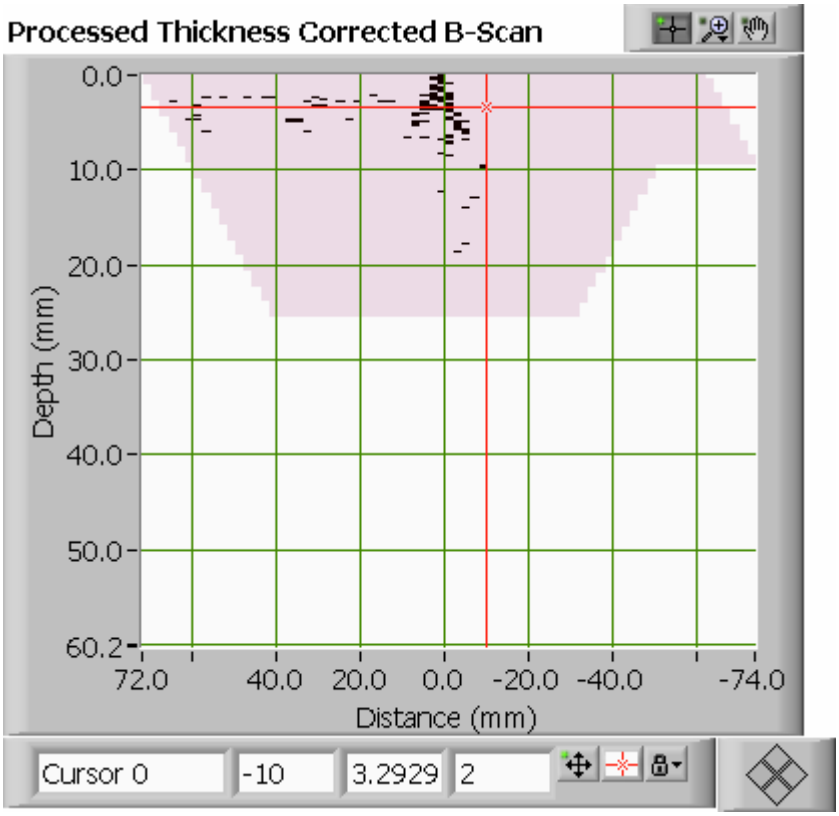


**Figure 1.4.1-18.** **Threshold-Processed Data** [The display showed a binary image, with 0 being the pink area, and 1 being the black (defected) data.]

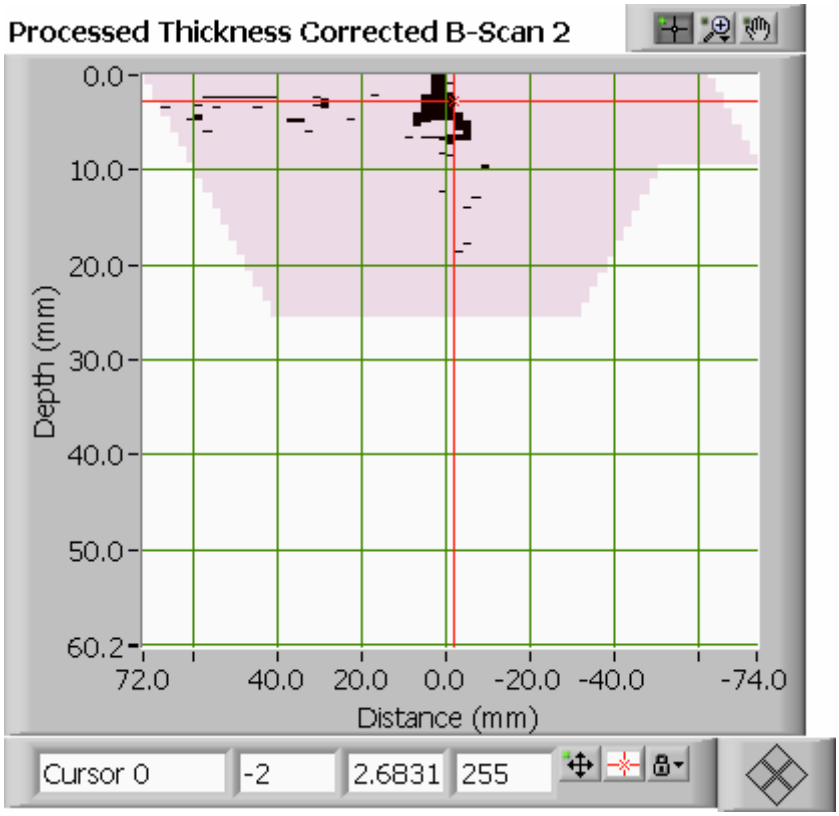


**Figure 1.4.1-19. Linked and Grouped Defect Data**

- **Numbering of Defects on Single B-Scan**

  - In this step, it is necessary to determine how many defects exist on one single B-scan in preparation for the further processing of data. An algorithm is developed that is similar to vision analysis routines for particles to determine the number of defect groups in a 2D data array as a basis of potentially linking all the defects within the same geometric regions across all B-scans.

- **Boundary Finding for Folded Data**

  - In this step, it is necessary to determine the points of the folded data such that correct "outer shell" of the scan coverage area can be correctly plotted. As stated earlier, the original groups of B-scans go through the data manipulation to re-position the data points back to their correct physical locations, and this step is to display and plot the boundary of this manipulation. It may also be possible for the future software to read in a 2½D CAD drawing of the part being inspected, and re-created a greater 3D wire frame data that enclose the folded data wire

frame. An example of the folded data boundary plot is shown in Figure 1.4.1-20. The end result of this step is the generation of point-cloud of all the boundary points that can be accepted by the 3D plotting routines for the regeneration of the scan coverage area.

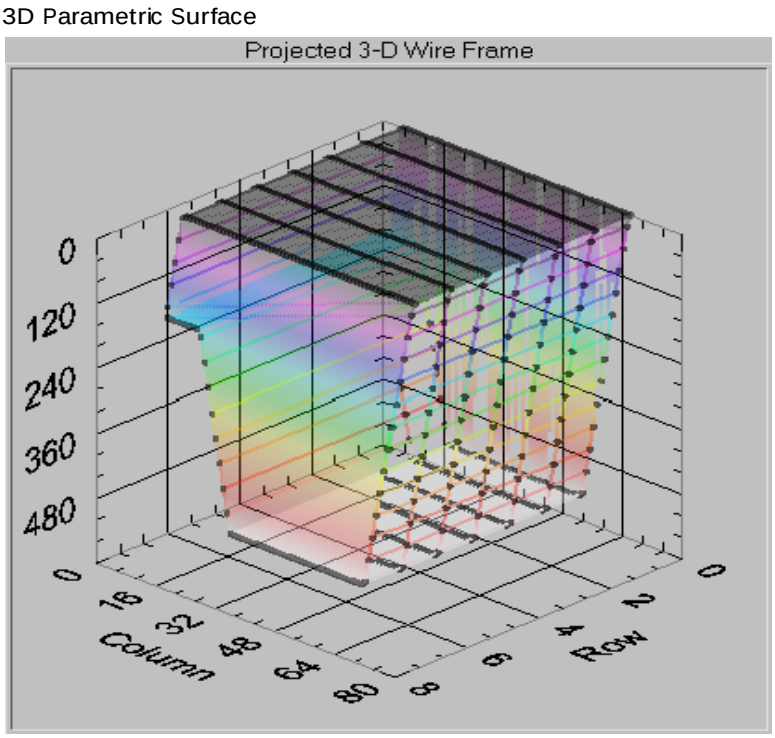


**Figure 1.4.1-20 3D Wire Frame of Folded Data Boundary**

- **Continuation of Defects in Groups**

  - Now that the individual groups of defects on one B-scan are all determined, it is necessary to see through all available B-scans to determine the extent of a certain defect through B-scans. The simplest form of this determination can be done using the following analogy: if the geometric boundary of a certain defect on one B-scan falls within the boundary of the defect on another B-scan, it is assumed that these two defects are in fact one spanning through these two B-scans. The same procedures will be performed recursively to seek the minimal number of defects (through overlap deduction), until all B-scans in the data file are processed. A separate memory location should be created to accommodate for all the coordinates for individual defect for further processing.

#### 1.4.1.2.12 Individual Defect Extension through B-scans

As stated previously, all the defect groups that spanned through multiple B-scans will be processed and number of defect reduced to a minimal set. The end result of this process is an multi-dimension array consists of every defects (starting from B-scan Number 1, but sometimes may start from B-scan Number n, as defects may be initiated somewhere in the middle) in terms of width, height, and starting geometric location on each B-scans.

##### 1.4.1.2.12.1 Boundary Generation for Individual Defect

After all of the individual defect extensions were found, the boundary information for each defect on each B-scan will need to be processed and retrieved. All of the coordinates on the defect will need to be determined, and extrapolated into a meaningful set of data points (point clouds) that is similar to the wire frame constituted by the boundary data set for the folded data. Note that the treatment of these sets of data may be quite different than that of the folded data set, as the geometric features presented in these data sets my be more complicated than that of the folded data.

*Defect Surface Generation (Iterations)*

As soon as all the point clouds are found, a polygon-like plotting algorithm is used to generate the “facets” of the defects that span through the B-scans. Note that further processing may still be needed to reduce the number of points in an effort to avoid plotting “internal” facets that do not appear to be on the defect surface.

*Overlaying of Generated Defect Groups into Bounded, Folded Data Frame*

When all the defect facets were well defined and generated, all the defects can then combined into the same plot as the boundary fold-back data. Note that the physical locations of the defects have to observe the physical coordinate constrains, e.g., all the defects have to be placed exactly as defined as individual B-scans, and the starting and ending positions also have to follow the results of all the prior algorithm calculations.

*Defect Generation and Plotting*

The last step in the representation of the defects in 3D is to plot all the defects together with the boundary. Note that in order to distinguish between the defects it may be necessary to plot various defects in different color. An example of the 3D defect representation may be shown in Figure 1.4.1-21.

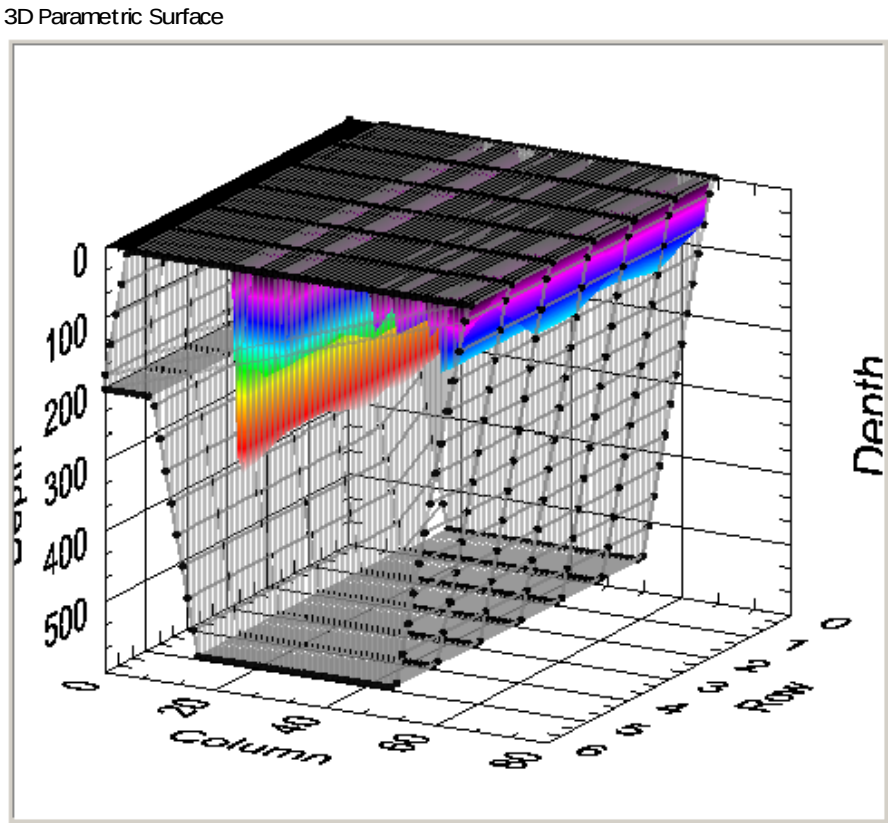


**Figure 1.4.1-21. An Exemplary 3D Representation of Defect Map**

*Future Work: Data Reduction*

It is foreseeable that additional work will need to be included to improve the performance of the algorithms, which will lead to a truly useful tool for inspectors in the fields to quickly and accurately determine the locations and orientation of defects, or even be able to size the defects accurately. Some of the focused areas are listed as follows:

- **Outlier Removal:** To remove some of the outliers that have the defect size of only one or two data points, which may be indicative that the data were noise in nature.

- **Part Geometry Input:** To acquire part information via some available CAD packages such as AutoCAD®, etc. It is foreseen that the most suitable format will be the 2½D, ASCII-compatible text file format (dxf file format) such that part geometry in one direction will be extended geometrically per defined. However, this approach may not work properly if the part geometry becomes complex, as the dimension cannot be extended readily with simple extension method.

- **Improved Data Merging:** This would be considered the major task in the future work. The basic working principles can be considered as follows: due to the nature of S-scans, the resultant data file will inevitably contain a lot of overlapped data (based on the angle projection of PA UT beams). It will be greatly beneficial to develop a methodology to remove the data redundancy while strengthening the defected data by verification through various S-scans. The end result of this analysis should provide an even better view of the actual defect map, with wider coverage area as additional coverage in the inspected areas were achieved through the electronic scanning of the PA probes.

#### 1.4.1.3 Conclusion

A methodology in representing PA UT inspection data in 3D has been investigated, and some promising results were found. Additionally, some of the filtering techniques that proved to be useful in real-work applications were also demonstrated. Further work is still needed to improve the performance of the algorithms. It is foreseen that this set of algorithms will be beneficial in assisting field personnel (inspectors, engineers, petrochemical organizations, etc.) to determine the severity of defects in the components quickly with visual representation.

#### 1.4.1.4 References


1.4.1-1. Savadjiev, P., Ferrie, F. P., and Siddiqi, K., “Surface Recovery from 3D Point Data Using a Combined Parametric and Geometric Flow Approach”, *Proceedings Energy Minimization Methods in Computer Vision and Pattern Recognition*, McGill University, Quebec, Canada (2003).

1.4.1-2. Amenta, N. and Kil, Y. J., “The Domain of a Point Set Surface”, *Proceedings Eurographics Symposium on Point-Based Graphics*, University of California at Davis (2004).

1.4.1-3. Pauly, M., Gross, M., and Kobbelt, L. P., “Efficient Simplification of Point-Sampled Surfaces”, *Proceedings of the Conference on Visualization*, ETH Zurich, pp. 163-170, ISBN: 0-7803-7498-3 (2002).

1.4.1-4. Lee, I. and Schenk, T., “3D Perceptual Organization of Laser Altimetry Data”, *Proceedings Int’l Archives of Photogrammetry and Remote Sensing*, Vol. XXXIV-3W4, The Ohio State University (October 2001).

1.4.1-5. Garland, M. and Heckbert, P. S., “Surface Simplification Using Quadric Error Metrics, *Proceedings SIGGRAPH ’97*, Carnegie Mellon University.

### 1.4.2 AUT Data Fusion and Improved Sizing and Analysis Techniques

The use of AUT data and techniques for advanced imaging and data fusion (data merging) are becoming increasingly more useful as computer processors become faster and data storage capabilities improve.[1.4.2-1] During the course of this project, various AUT imaging and AUT data-combining (data fusion) techniques were evaluated to determine their effectiveness for improving flaw detection and sizing. This section gives a basic explanation of popular AUT imaging techniques, as well as recent advancements that can be beneficial for girth weld inspection.

In the past, UT inspectors relied only a real-time A-scan display (lower left corner of Figure 1.4.2-1) to view weld inspection data. While the basic inspection data was virtually the same as that collected today, the quality of the inspection was largely dependent on the skill level of the inspectors, with no method of reviewing inspection data after the inspection was completed. After an inspection, the inspection records contained only written notes describing what was found during the inspection and the location, length, depth, and amplitude of any recordable indications. The location and length of UT indications were dimensioned using a scale to physically measure the distance that the transducer was moved from one point along the weld to another point. The depth of indications was read from the time baseline of the A-scan display, and signal amplitude, rather than flaw height, was used as the primary measure of flaw severity. In contrast, the use of today's AUT systems not only allows inspection data to be archived for future reference, but also makes the data easier to view and analyze.

Typically, the three pieces of data are collected during an AUT weld scan are: signal amplitude reflected from ultrasonic reflectors, TOF to ultrasonic reflectors, and probe position. Using these three pieces of data, images can be constructed to view the data. When collected data is combined with inspection parameters such as material sound velocity, part thickness, and sound beam angle; software tools, such as linked cursors, can then be used to measure flaw height, length, and depth directly from the imaged data.

Some of the more popular data imaging techniques which have been widely used for many years are A-, B-, C-, and D-scans. In addition to these data viewing techniques, PA offers a S-scan view which is made possible through electronic steering of the sound beam through a range of angles. The S-scan is familiar to many people as the wedge shaped display often seen in medical ultrasound. Following is a brief explanation of each ultrasonic data display technique.

[1.4.2-1] Edited by Gros, X. E., *Applications of NDT Data Fusion*, Kluwer Academic Publishers (2001).

- **A-Scan –** is the basic ultrasonic waveform data displayed as amplitude of the reflected sound energy versus the TOF of the ultrasonic wave.

- **B-Scan –** is a graphical representation of the ultrasonic data where the TOF of the ultrasonic wave is plotted against the probe travel position. For weld inspection it is normally a cross-sectional view across the weld at a specific location.

- **C-Scan –** is a graphical representation of the ultrasonic data where the amplitude of the reflected ultrasonic wave is plotted against the X-Y position of the probe (a plan view).

- **D-Scan –** (same as B-scan except rotated 90 degrees) is a graphical representation of the ultrasonic data where the TOF of the ultrasonic wave is plotted against the probe travel position. For weld inspection it is normally a cross-sectional view along the weld length.

- **E-Scan –** is a new expression for an electronic raster B-scan at fixed angle.

- **S-Scan –** is a graphical representation of PA ultrasonic data where multiple angles of TOF data are corrected for sound path differences and displayed from a single probe location.

- **Polar View –** is a 2D graphical representation of UT data from inspection of cylindrical parts that provides information of defect location (ID/OD depth and angle) if it is used in conjunction with the 2D girth weld layout.

An example of the most popular display formats are shown in Figure 1.4.2-1.

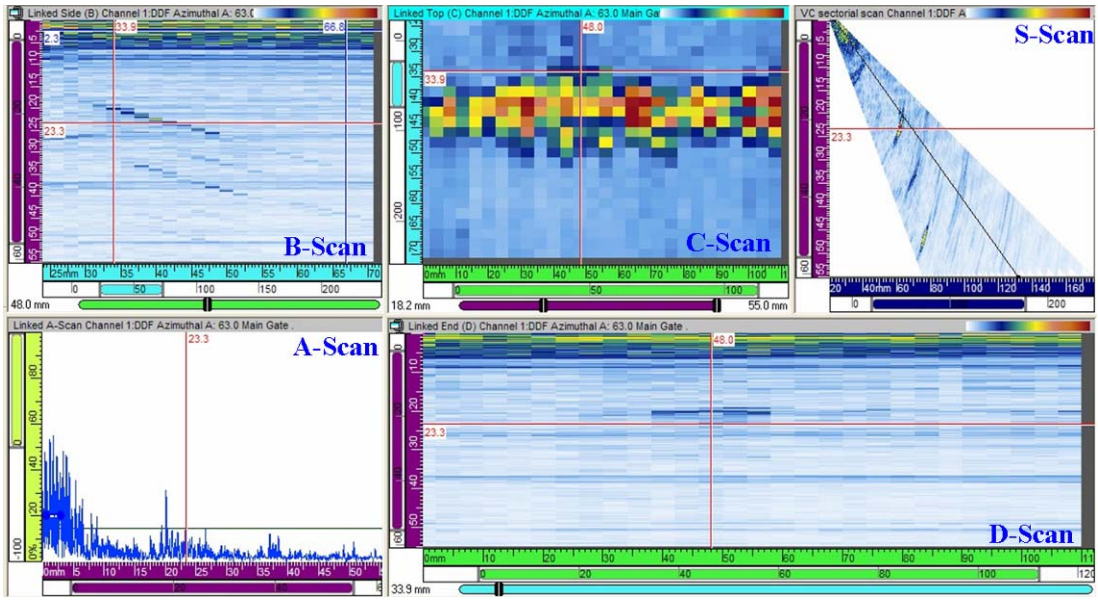


**Figure 1.4.2-1. Example of UT Data Display Techniques**

The use of multiple displays such as the one shown in Figure 1.4.2-1, can allow a large amount of data to be viewed quickly. For example, using a C-scan, it can quickly be determined if any indications were detected in the entire scan area. If so, the B- and S-Scans can be used to provide information regarding flaw depth and height, while the D-scan will provide information about the length of the flaw. The S-scan can be further used to select the best beam angle for viewing a particular flaw. If the data views are linked, changing the beam angle in the S-scan will result in the data for the selected angle being displayed in the other views.

As a result of being able to electronically steer and focus the beam, a sectorial, or azimuthal, scan [Figure 1.4.2-2 (right)] can be generated as a real-time side view from a single inspection point without any physical motion from the PA transducer. The direct relationship between the location and size of the flaws in the S-scan image can assist interpretation. For example, when inspecting a crack, sectorial scanning can allow a simultaneous look at both the root and tip of the crack [Figure 1.4.2-2 (left)]. From this display, the height of the crack can be measured with higher accuracy by manipulating the ultrasound beam electronically.

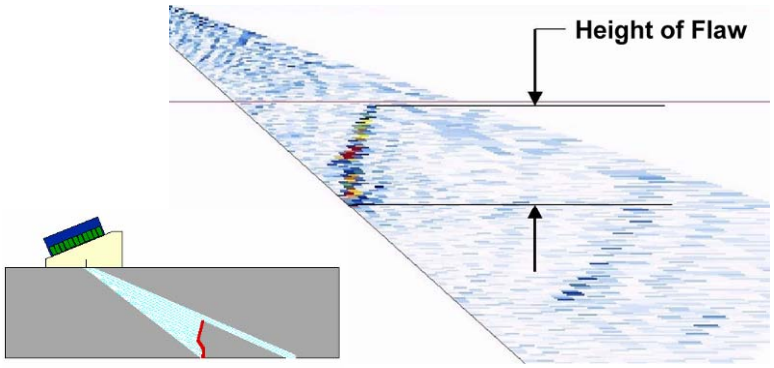


**Figure 1.4.2-2. Proposed Time-Based Sizing of a Crack Using PA UT**

Typically, data collected using PA raster scanning was well suited for data fusing. Based on AUT-PA scans performed during this project, it was found that displaying multiple beam angles in a fused D-scan format helped to quickly locate flaws and also get a quick estimate of the length and height of each flaw. This was accomplished by merging (fusing) all the scan data for each beam angle. Figure 1.4.2-3 shows an example of fused D-scan views for five different beam angles (45, 50, 55, 60, and 65 degrees) along the entire weld length of a 61.0-cm (24-in.)-diameter pipe having a 7.8-mm (0.31-in.) wall thickness. In Figure 1.4.2-3 the horizontal axis is distance along the weld and the vertical axis is material depth.

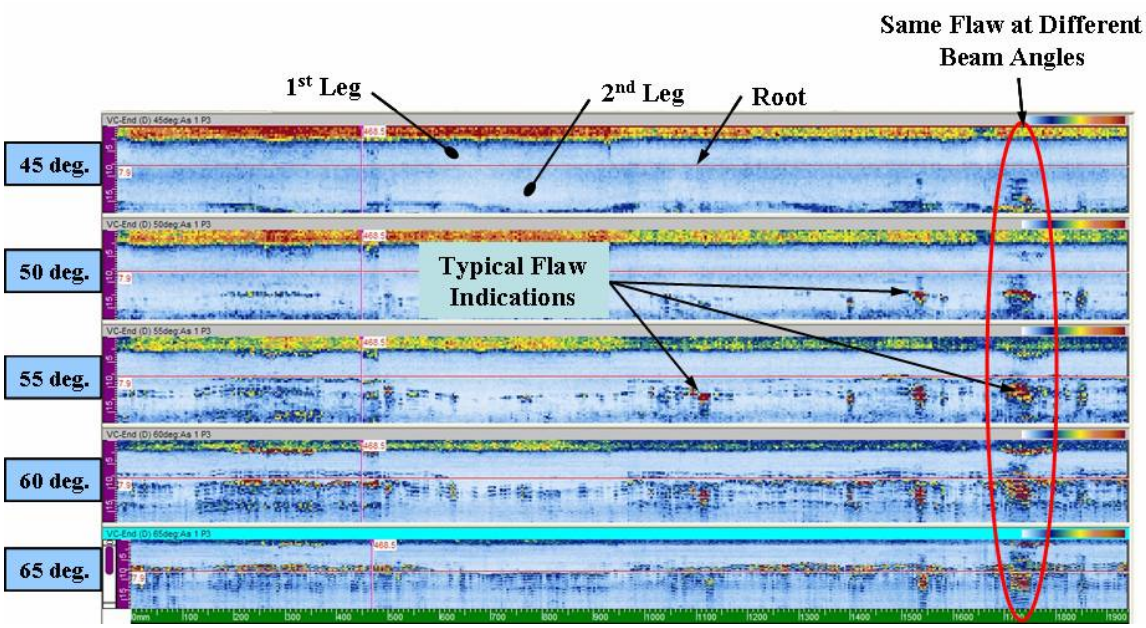


**Figure 1.4.2-3. Fused D-Scan Views of 61.0-cm-Diameter Girth Weld**

Another methodology for displaying PA data is by the use of a multi-angle D-scan view. This was found to be particularly good for determining the through-wall dimension of flaws. For this application, scan data from each angle of the sector scan was combined into a single view with all the data corrected for the different sound paths for each angle used. Specifically, this technique proved helpful for determining the through-wall height of fatigue cracks discussed in Section 1.6.4 of this report. Figure 1.4.2-4 shows an example of a multi-angle D-Scan view from a through-wall fatigue crack. The image was created by merging angle beam shear wave data of 45 to 70 degrees in 1-degree steps. By using this technique, it was possible to get an idea of the overall shape of the crack which, in turn, was helpful for determining the length of the crack on both the OD and ID surfaces.

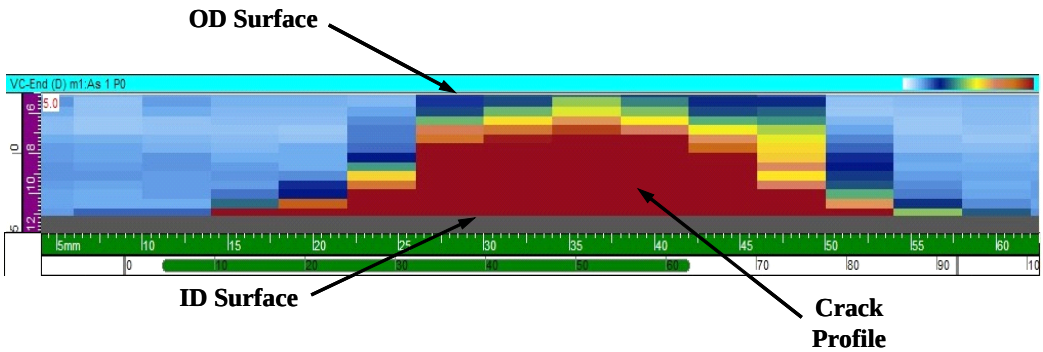


**Figure 1.4.2-4. Multi-Angle D-Scan View of a Through-Wall Fatigue Crack in 11.7-mm (0.46-in.)-Thick Pipe Wall**

Data fusion is beneficial when it is desirable to combine different data into one view. Figures 1.4.2-5 through 1.4.2-13 show different possibilities for fusing PA data. All data shown in Figures 1.4.2-5 through 1.4.2-13 were collected from two PA raster scans (one US scan and one DS scan) on a 60.1-cm (24-in.)-diameter pipe girth weld with a 13.8-mm (0.54-in.) wall thickness. Figures 1.4.2-5 and 1.4.2-6 show the US and DS fused D-scans, respectively, for five beam angles. Figure 1.4.2-7 is a complete polar view which is basically a circular D-scan. Figure 1.4.2-8 is a zoomed location on the same polar view showing how weld flaws can be viewed.

Figures 1.4.2-9 through 1.4.2-13 show a progression of how a large amount of data can be fused and imaged. Figures 1.4.2-9 and 1.4.2-10 show multi-angle D-scan views of the US and DS scans, respectively. The first leg data is in the upper half of each view and the second leg data is in the lower half. When using these views, it is possible to determine which flaws were detected on the US scan and which were detected on the DS scan. In Figures 1.4.2-11 and 1.4.2-12 the second leg data for the same US and DS scans have been folded up onto the first leg data to give a combined view. Figure 1.4.2-13 goes one step further by merging the US and DS scan data together into a single view.

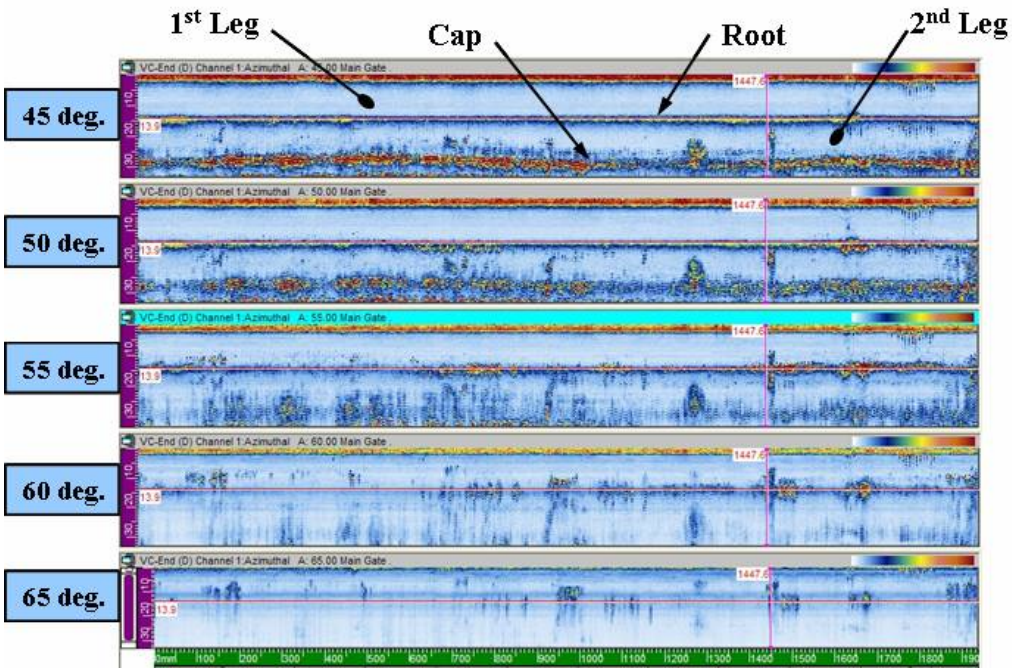


**Figure 1.4.2-5. Fused D-Scan Views for US Scan**

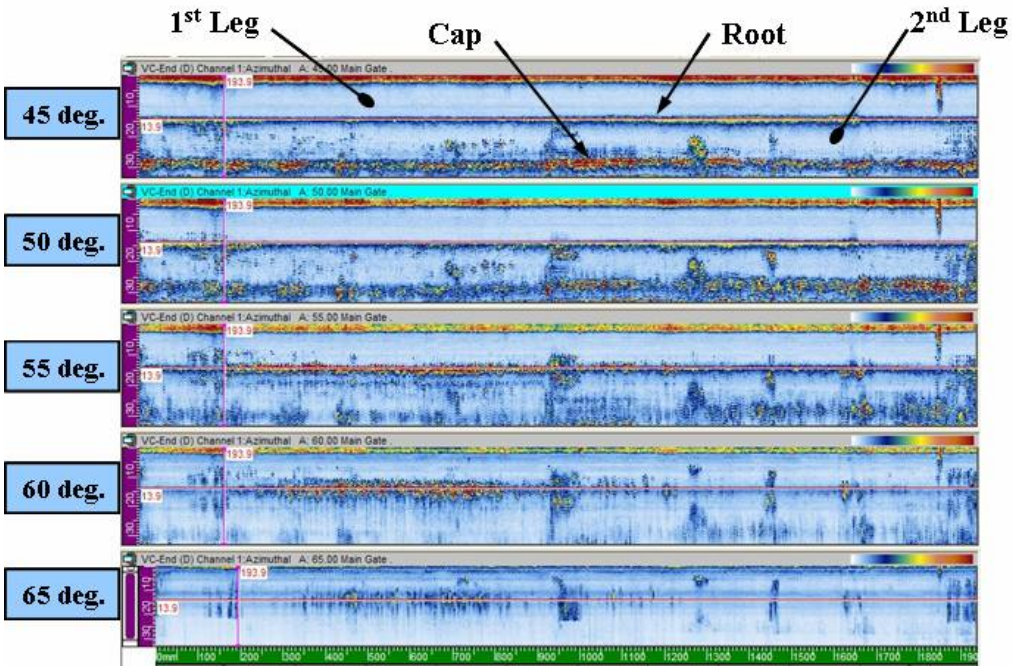


**Figure 1.4.2-6. Fused D-Scan Views for DS Scan**

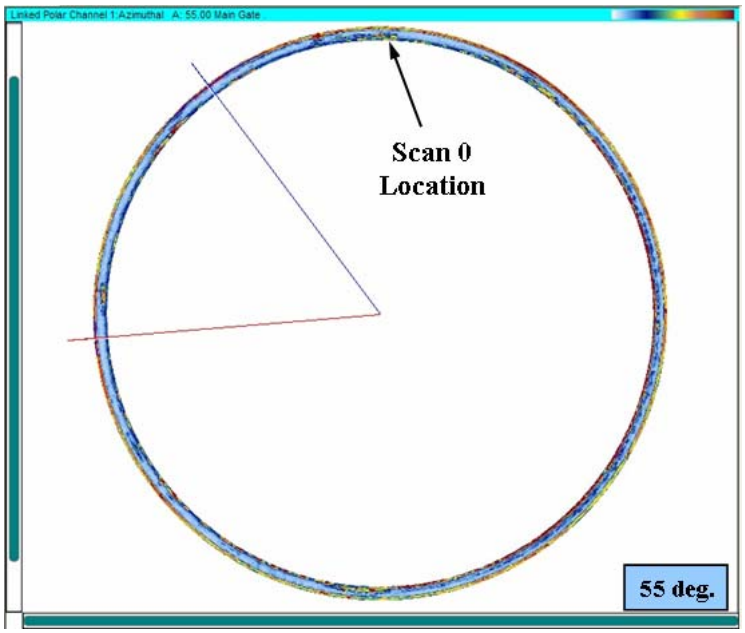


**Figure 1.4.2-7. Polar View for DS Scan**

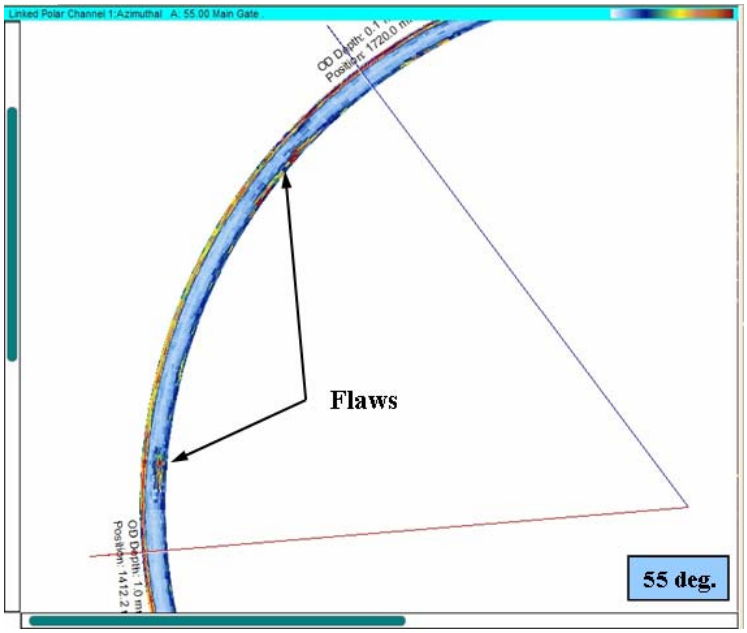


**Figure 1.4.2-8. Zoomed Polar View for DS Scan**

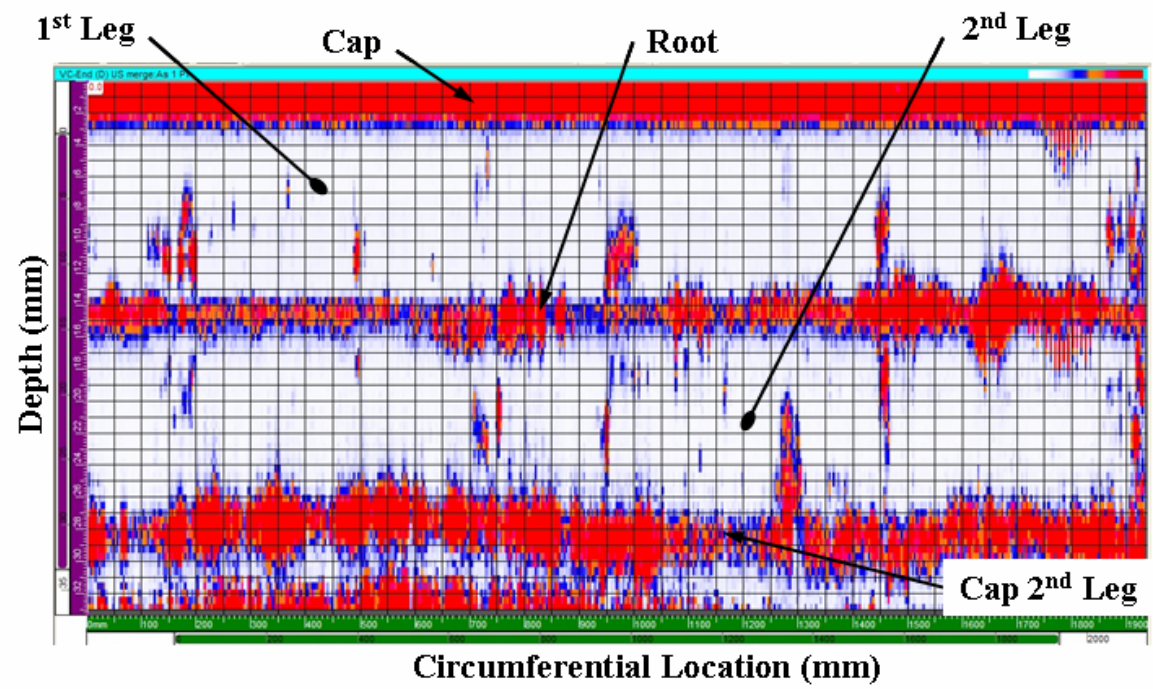


**Figure 1.4.2-9. Multi-Angle D-Scan View for US Scan**

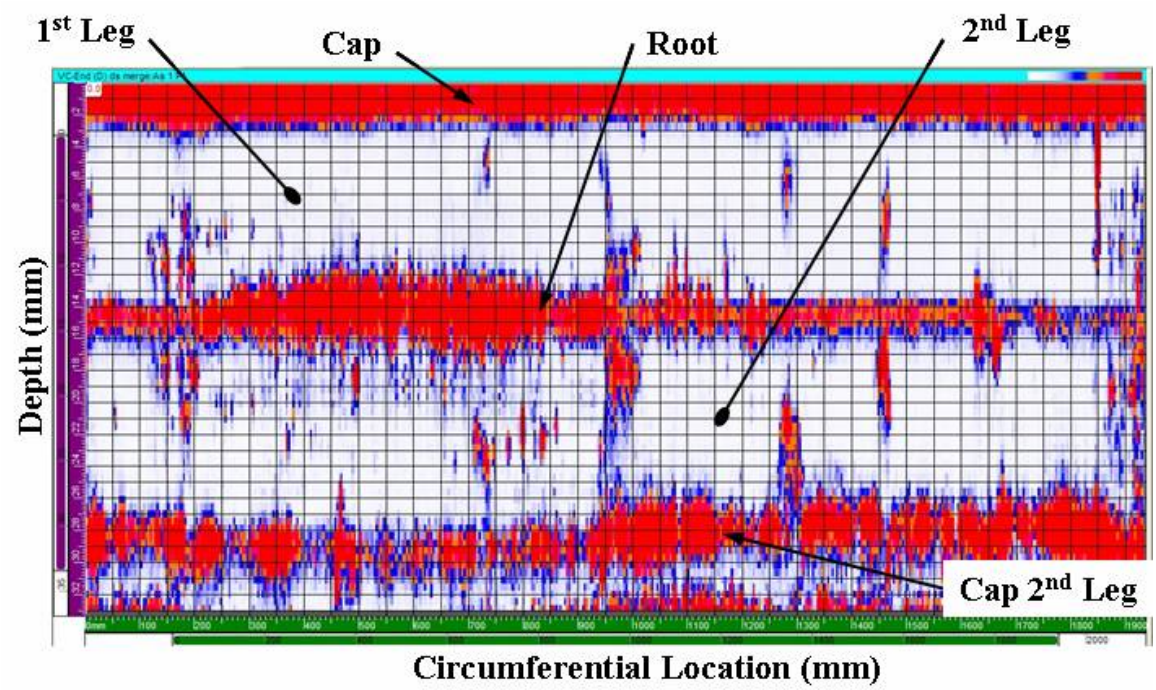


**Figure 1.4.2-10. Multi-Angle D-Scan View for DS Scan**

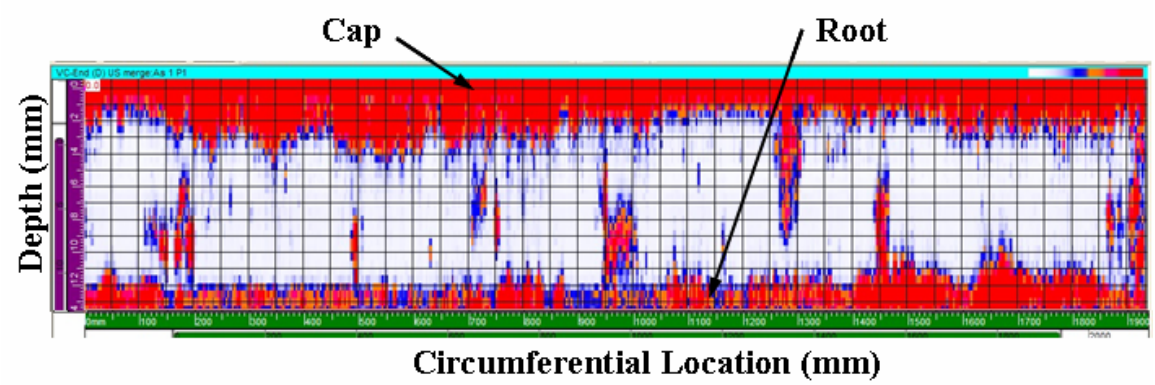


**Figure 1.4.2-11.** **Multi-Angle D-Scan View for US Scan with Second Leg Folded up on First Leg**

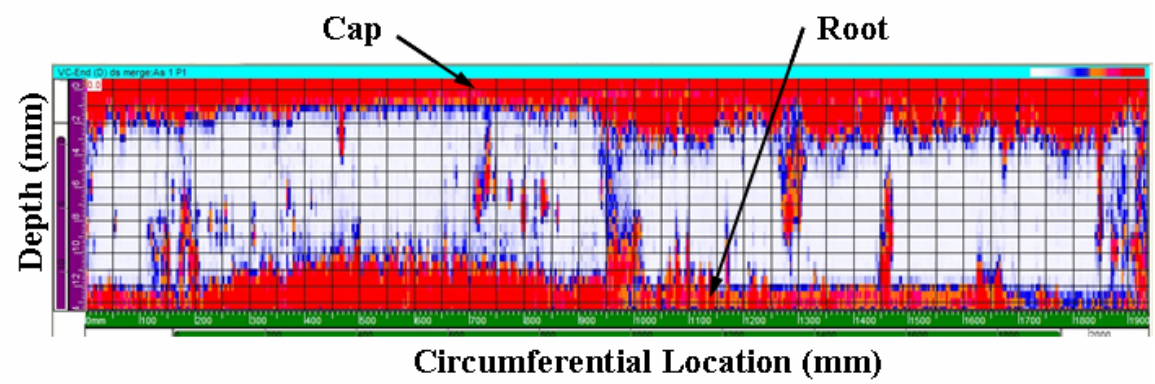


**Figure 1.4.2-12.** **Multi-Angle D-Scan View for DS Scan with Second Leg Folded up on First Leg**

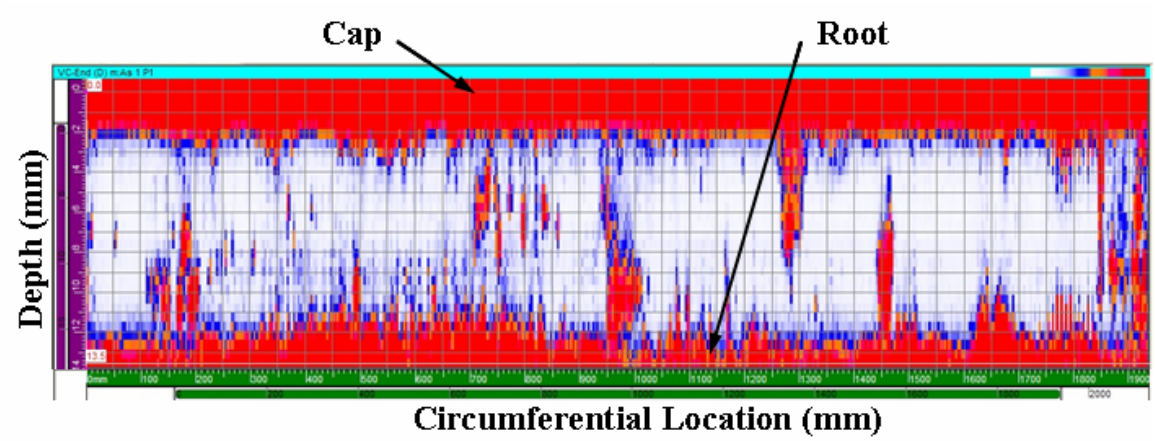


**Figure 1.4.2-13.** **Multi-Angle D-Scan View with US and DS Data Fused and Second Leg Folded up on First Leg**

For sizing individual flaws it was found that the S-scan view was good for determining flaw height. An S-scan can be used in conjunction with other views such as A- and B-scan views to measure signal amplitude or to help locate and confirm the extent of an imaged signal. Figure 1.4.2-14 shows flaws on the US and DS bevel of a girth weld as the beam angles are electronically steered from a single probe location.

The choice of how the data is combined and viewed would be determined by the level of detail needed. For example, to determine the absence or presence of flaws and their approximate size, the combined US and DS multi-angle D-scan view in Figure 1.4.2-13 could be used. If one wanted to see just flaws detected from the DS scan, the multi-angle D-scan shown in Figure 1.4.2-10 could be used. If more accurate location or sizing information is needed, a different view such as that shown in Figure 1.4.2-14 would be used. However, in every case the views could be generated from the same scan data without need for re-scanning the weld.

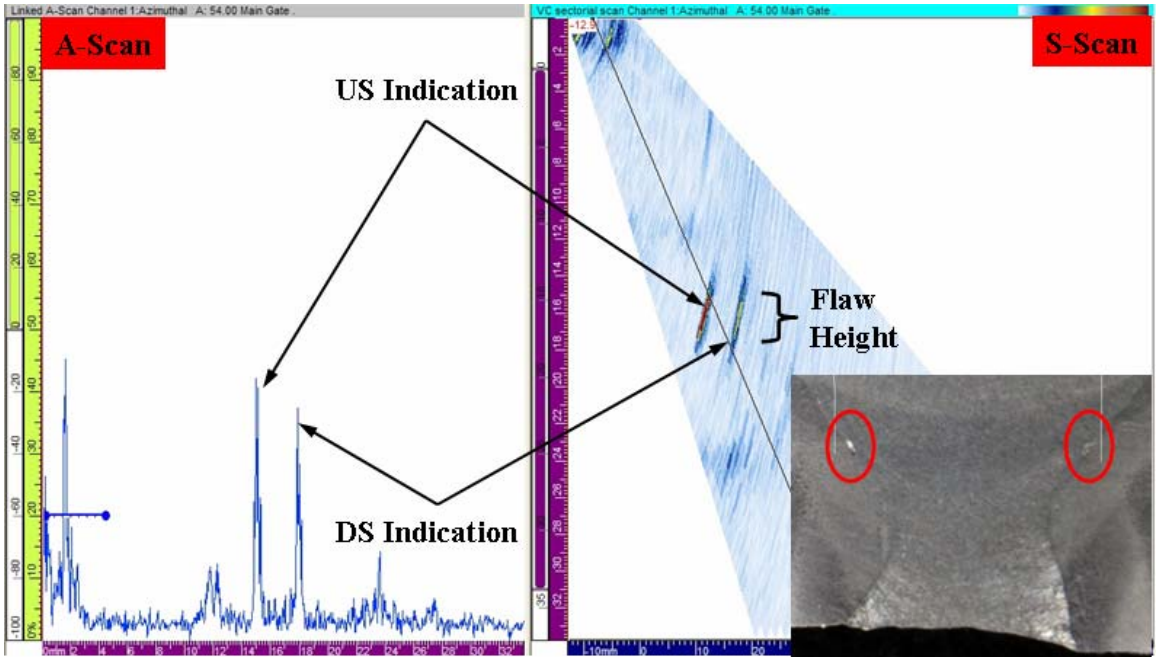


**Figure 1.4.2-14. A- and S-Scan Views of Flaws on the US and DS Weld Bevels**

It was found that the use of data merging or data fusion techniques greatly enhanced the ability to determine the location and size of flaws. For example, the use of a polar view helped to visualize the circumferential locations of flaws and the through-wall extent. It was also found that by merging data from the different beam angles collected, it was possible to get a composite view of the weld.

Reconstruction of the defects using fused (merged) AUT images was able to enhance defect localization, improve defect shape identification, help to identify the cause of the flaw, and provide complimentary information for ECA engineers. The improved imaging created conditions for replacement of the traditional zone height amplitude-based approach by a novel time-based approach where combine AUT information is reconstructed from multiple A-, B-, D-, and S-scan images and polar views generated by AUT systems using linear PA probes and applying electronic beam focusing, steering, and scanning. Therefore, additional powerful capabilities can be added to the current 2D strip charts.

### 1.4.3 Establishing Improved Ultrasonic Test Sensitivity Levels

During this project EWI looked at current calibration reference reflectors and the UT techniques used, to determine if improvements could be made that would make UT weld inspection better and more reliable. An adequate UT test sensitivity level is crucial for proper flaw detection. Consequently, if the calibration reflector is not of the appropriate type and size, it can result in the sensitivity level being too low or too high. Either situation can be detrimental to obtaining good detection and sizing information.

Review of inspection procedures from UT vendors showed that 1.0- × 10-mm (0.04- × 0.39-in.) notches are typically used for establishing gain settings for inspecting the weld root, and 2- or 3-mm (0.08- or 0.12-in.)-diameter FBHs are typically used for the root land/lack of complete penetration (LCP) and weld bevel regions. Calibration reference reflector type and size is often given as a range or not specified at all in industry standards and is usually left to the discretion of the UT vendors. While UT vendors can often select reference reflectors they feel are appropriate this does not mean that there is a lack of control in establishing test sensitivity. Many standards require UT vendors to demonstrate that their UT procedures will detect and accurately size flaws that do not meet the acceptance criteria. The demonstration/validation is generally performed on mockup samples containing flaws of various types and sizes which must be detected and accurately sized by the UT vendor.

In order to evaluate the differences in calibration blocks and various reflectors used, EWI gathered experimental comparison data from standard calibration samples, custom calibration samples, as well as typical calibration samples fabricated by AUT vendors for girth weld inspection in accordance with ASTM E-1961. Ultrasonic techniques used for the comparisons were typical of those used for girth weld inspection. For example, OD, ID, and LCP zones were evaluated using P/E techniques, while weld bevel zones were evaluated using tandem pitch-catch techniques. Experimental data was collected to look at the UT test sensitivity difference when using various size notches, as well as notches that were tilted. Test sensitivity differences were also measured for both 2- and 3-mm (0.08- or 0.12-in.) FBHs typically used to detect side-wall fusion flaws. Comparisons were also made between identical calibration blocks made by different vendors. Lastly, experimental data was collected to compare the signal amplitude response of notches, FBHs, and 1.2-mm (0.047-in.)-diameter SDH.

The baseline calibration reference sample used by EWI for this project was a NAVSHIPS block which is a commercially available carbon steel reference sample containing a series of 1.2-mm (0.047-in.)-diameter SDH. The holes range in depth from 6.4 to 69.9 mm (0.25 to 2.75 in.). For this project, the 19.1- and 25.4-mm (0.75- and 1.0-in.)-deep holes were used for establishing test sensitivity and for depth calibration. The ultrasonic instrument gain was adjusted so that

the reflected signal from the 1.2-mm SDH hole was set at 80% of FSH. The 19.1 mm (0.75 in.) was used for establishing the gain setting when the pipe wall thickness was less than 9.5 mm (0.38 in.) while the 25.4-mm (1.0-in.)-deep hole was used when the wall thickness was greater than or equal to 9.5 mm (0.38 in.). Normally, 6 to 10 dB was added to this value for scanning depending on the noise level. This gain level was chosen in order to obtain a relatively high sensitivity inspection, one that was higher than the sensitivity levels typically used for current girth weld inspection.

Two custom reference samples were fabricated by EWI to evaluate P/E techniques normally used for inspection of OD, ID, and LCP weld zones. These were identified as EWI-1 and EWI-2. Calibration Sample EWI-1 was fabricated from a section of 40.6-cm (16-in.)-diameter pipe having a 24-mm (0.94-in.) wall thickness. A sketch of this calibration reference sample is shown in Figure 1.4.3-1. This pipe calibration sample had five notches on the ID surface of the pipe and one 3-mm-diameter FBH drilled parallel to the pipe surfaces to simulate fusion flaws in the LCP area. The notches were 1-mm wide × 10-mm long with the notch heights ranging from 0.5 to 2.5 mm in 0.5-mm increments. The purpose of this sample was to compare gain settings established on 1.2-mm-diameter side-drilled reference holes to FBHs and notches typically used for establishing test sensitivity for girth weld inspection.

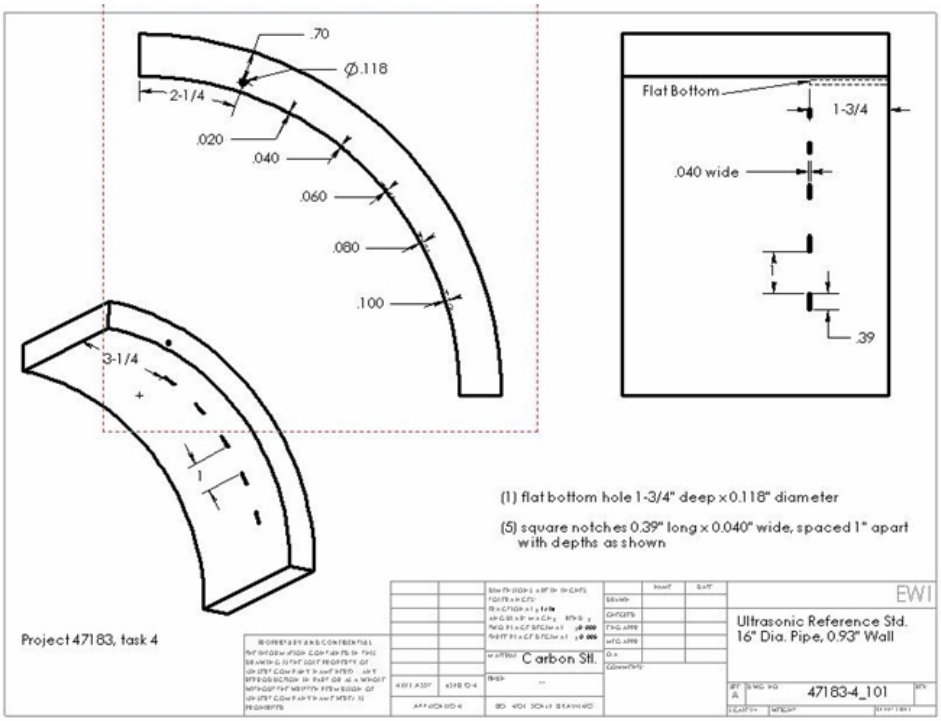


**Figure 1.4.3-1. EWI-1 Calibration Reference Sample**

The EWI-1 calibration reference was scanned using P/E techniques at scanning gains established from the 1.2-mm (0.047-in.) SDH. After scanning, experimental data was normalized so that the reflected signal from a 1.2-mm SDH at 25.4-mm deep was at a relative amplitude value of 0 dB. Results graphed in Figure 1.4.3-2 show typical trends between reflected signals received from reference notches having through-wall heights in the range of 0.5 to 2.5 mm when inspected using beam angles from 45 to 65 degrees.

Following are observations made from experimental results obtained from calibration sample EWI-1:

- Signal amplitude tended to increase as notch height increased; however, the increase was not linear.
- Lower beam angles produced higher signal amplitudes from the notches than did higher beam angles.
- When compared to the 1.2-mm SDH, the reflected signal amplitude from the 3-mm FBH averaged approximately 10 dB lower than the reflection from the 1.2-mm SDH.
- Reflections from the 3-mm FBH came from the edges of the hole rather than the flat bottom face (Figure 1.4.3-3).

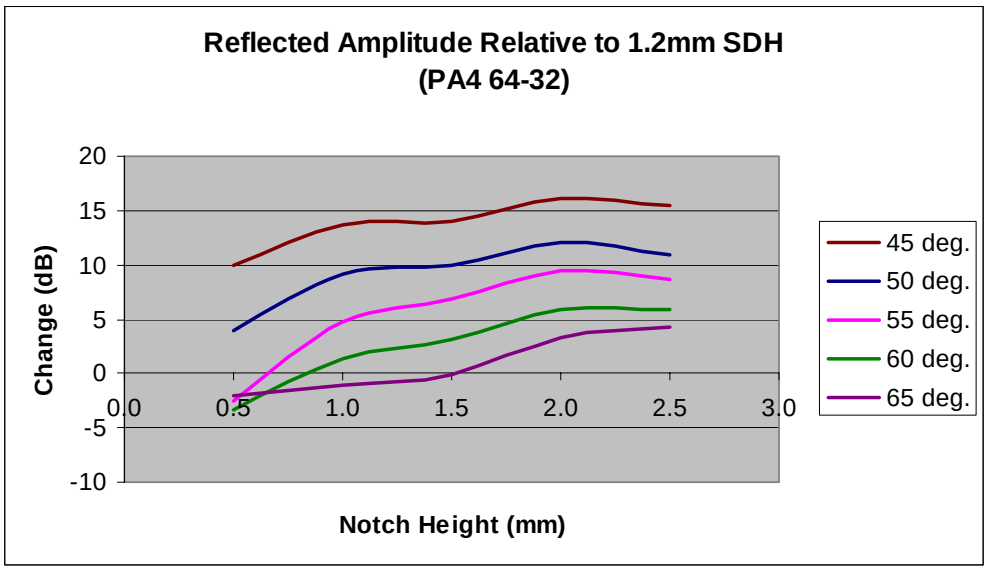


**Figure 1.4.3-2. Comparison of the Reflection from a 1.2-mm SDH Compared to 10-mm-Long Notches with a Range of Through-Wall Heights**

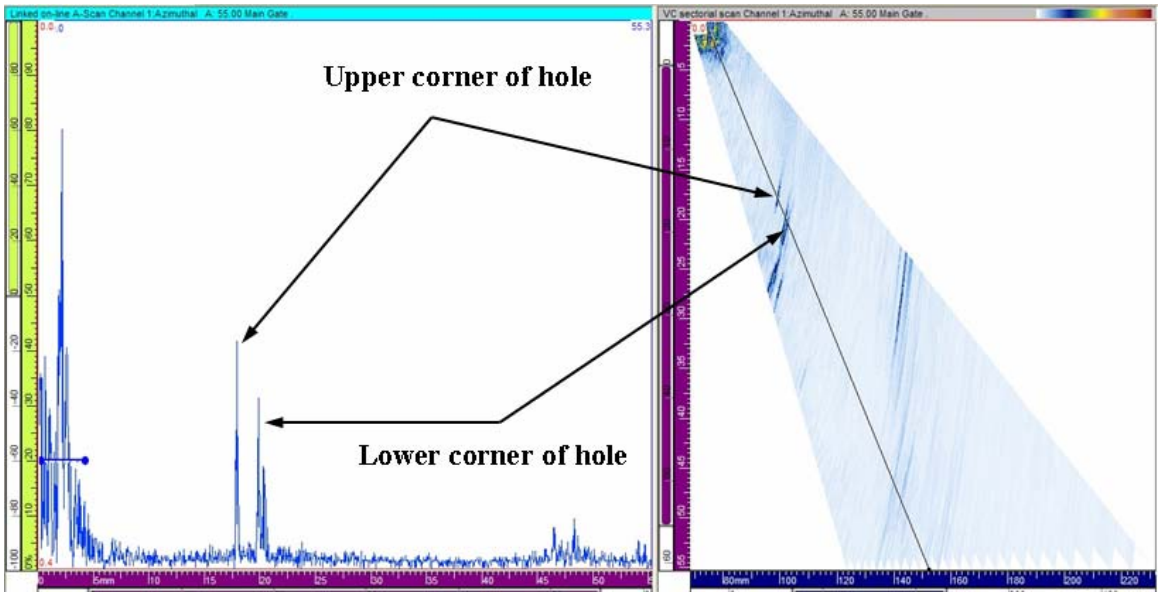


**Figure 1.4.3-3. Typical Reflected Signal from the Face of a 3-mm FBH used for LCP Zone in Calibration Sample EWI-1**

Calibration Sample EWI-2 was a 40.6-cm (16-in.)-diameter pipe with a 31.8-mm (1.25-in.) wall thickness. The sample was designed and fabricated to evaluate both OD and ID notch response from notches having dimensions in the ranges of 0.5 to 1.5 mm (0.02 to 0.06 in.) in height and 5.0 to 10.0 mm (0.20 to 0.39) in length. All notches were 1.0 mm (0.04 in.) in width. Inclined and non-inclined EDM notches were fabricated in both the longitudinal and circumferential directions of Sample EWI-2. All inclined notches were either 1.0 or 1.5 mm (0.04 or 0.06 in.) in height and were tilted at a 10-degree angle. For all notches, there was distance of 15 mm (0.59 in.) between the end of one notch and the beginning of the next. Figure 1.4.3-4 is a sketch of the calibration sample as machined.

After fabricating the calibration sample, PA UT techniques were developed using the EDM reference notches. Since notches of this type are often used for establishing sensitivity levels for OD and ID surface-breaking flaws, it is important to have techniques that will provide adequate detection. Despite the relatively heavy wall thickness, it was possible to develop all techniques using a 60-element, 7.5-MHz, PA probe with 32 active elements. Electronic steering and focusing were used to steer the sound through multiple beam angles and to focus the sound energy on the OD and ID surfaces.

Generally, ultrasonic beam angles of 45 to 60 degrees are used for detection of OD and ID flaws. The results for this diameter and wall thickness showed that the best beam angles for detecting notches perpendicular to the longitudinal axis of the pipe (such as those used for

detection of girth weld flaws) were angles in the 38- to 48-degree range. However, the best beam angles for detecting notches parallel to the longitudinal axis of the pipe (such as those used for detection of longitudinal seam weld flaws) were angles in the 30- to 40-degree range. The lower angles required for notches parallel to the longitudinal axis is due to the pipe curvature and wall thickness and would change depending on the OD-to-ID ratio of the pipe being inspected. Angles in the 30- to 40-degree range actually intersect the radial axis of the pipe at angles of approximately 36 to 50 degrees. Figure 1.4.3-5 shows that for the curvature and wall thickness of Sample EWI-2, a 40-degree beam angle intersects the radial axis at a 49.63-degree angle. This would be similar to using a 49.63-degree angle for detection of a back surface notch on a flat plate.

All notches in Sample EWI-2 were readily detectable within the angle ranges noted above. This includes the smallest notches having dimensions of $0.5 \times 5$ mm, as well as notches inclined at a 10-degree angle. Further, the notches were easily identified as separate notches even though the probe width was nearly as wide as the spacing between notches. The probe elements were 10-mm (0.39-in.) wide in the passive beam axis and the notches were only 15 mm (0.59 in.) apart. Figures 1.4.3-6 through 1.4.3-9 show scan results of the notches in Sample EWI-2.

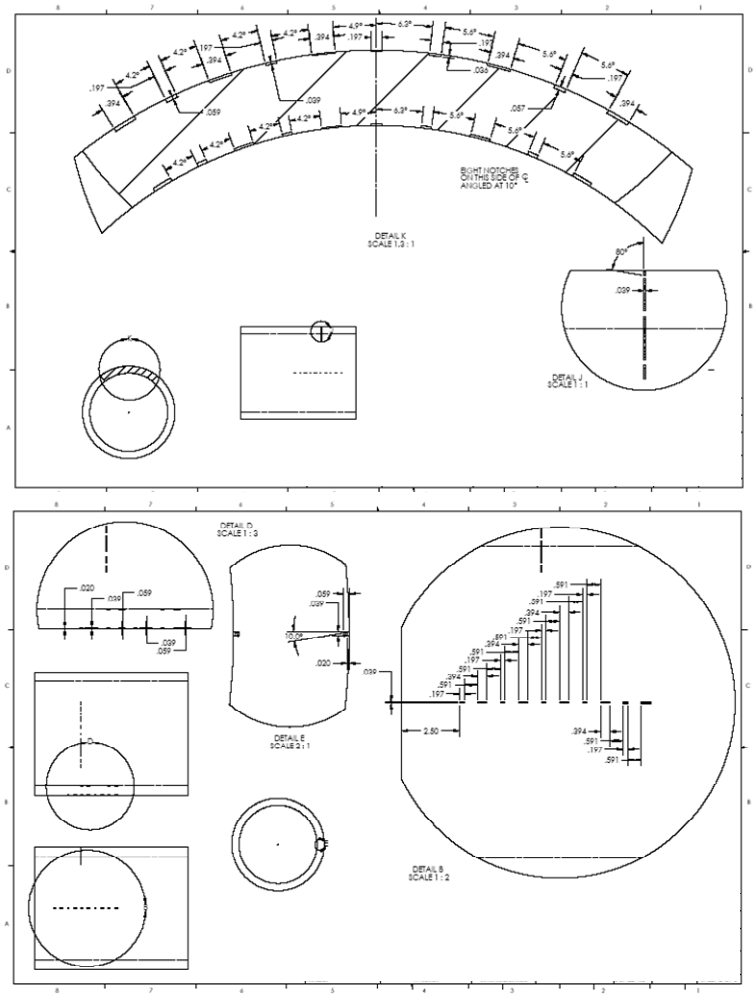


**Figure 1.4.3-4. EWI-2 OD and ID Notch Calibration Sample**

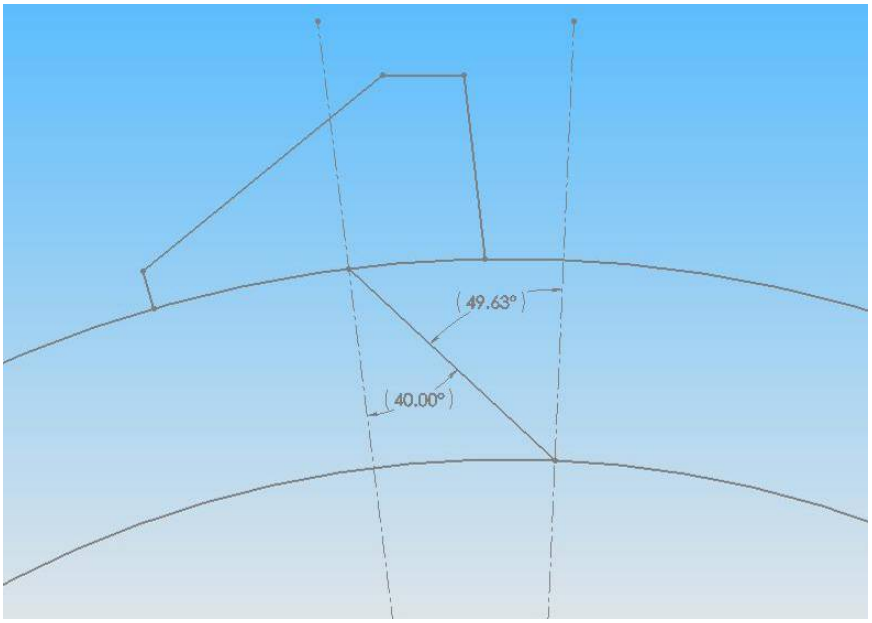


**Figure 1.4.3-5. 40-Degree Beam Angle Intersecting Radial**

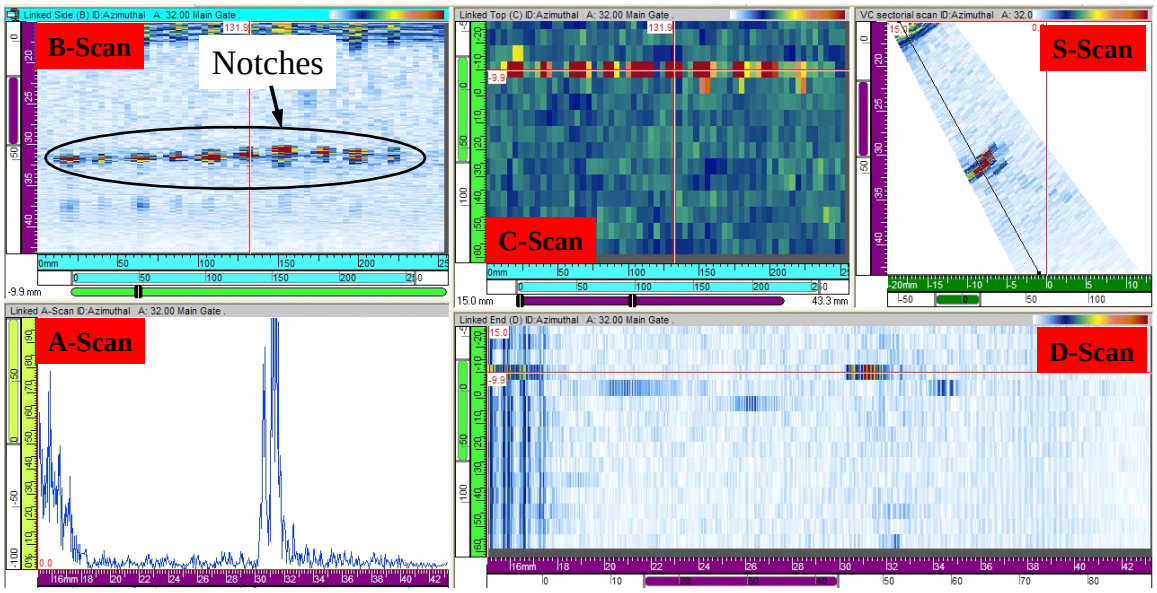


**Figure 1.4.3-6. PA AUT Scan of ID Notches Oriented Parallel to the Longitudinal Pipe Axis**

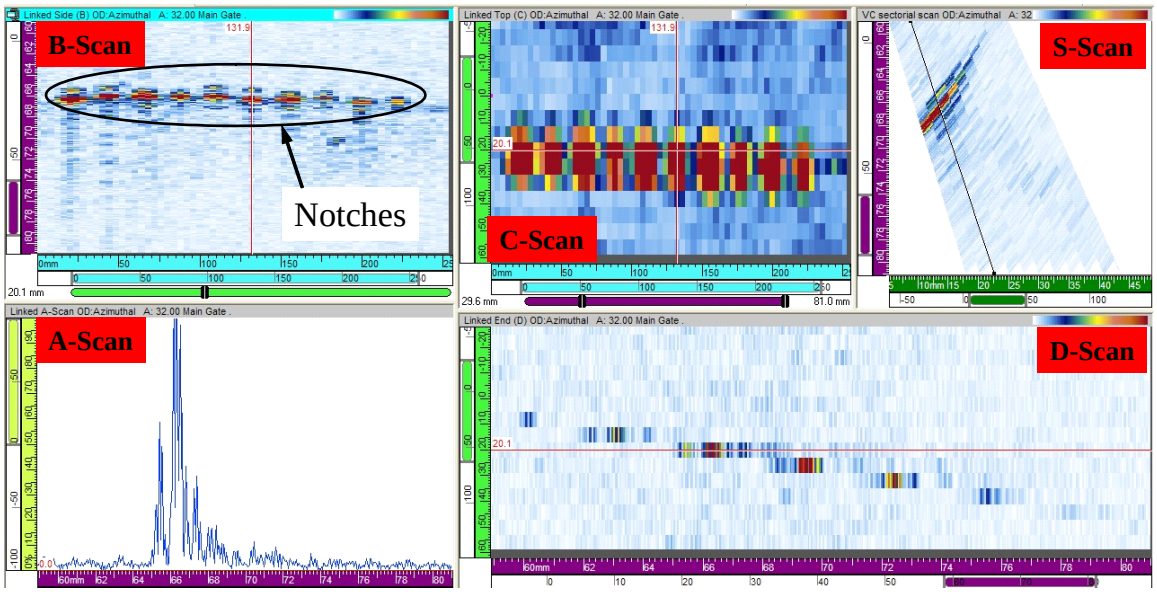


**Figure 1.4.3-7.** **PA AUT Scan of OD Notches Oriented Parallel to the Longitudinal Pipe Axis**

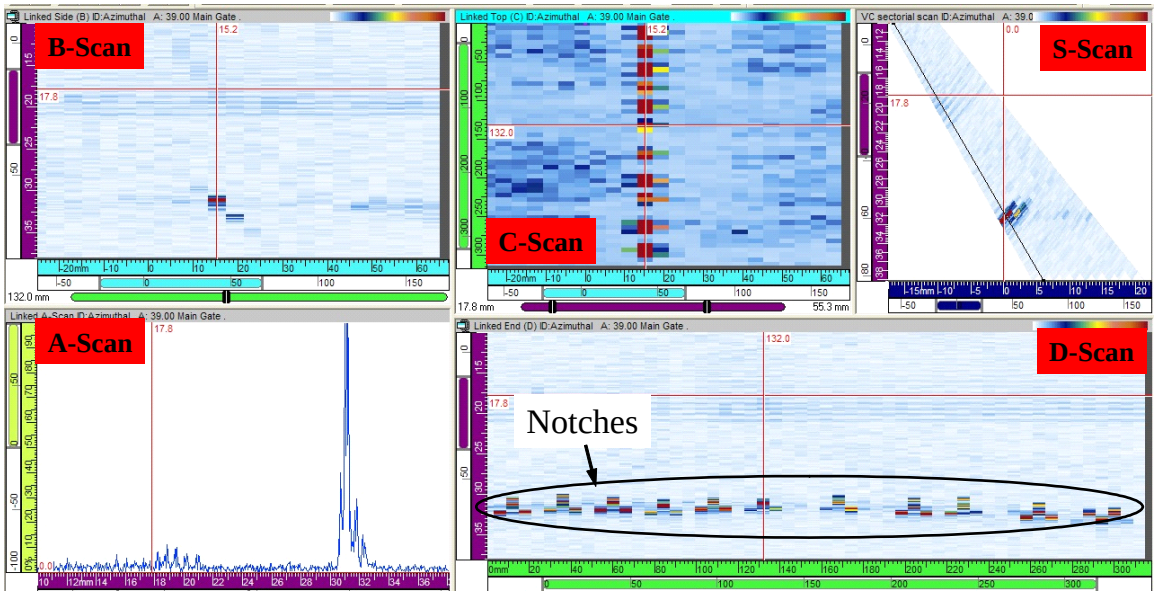


**Figure 1.4.3-8.** **PA AUT Scan of ID Notches Oriented Perpendicular to the Longitudinal Pipe Axis**

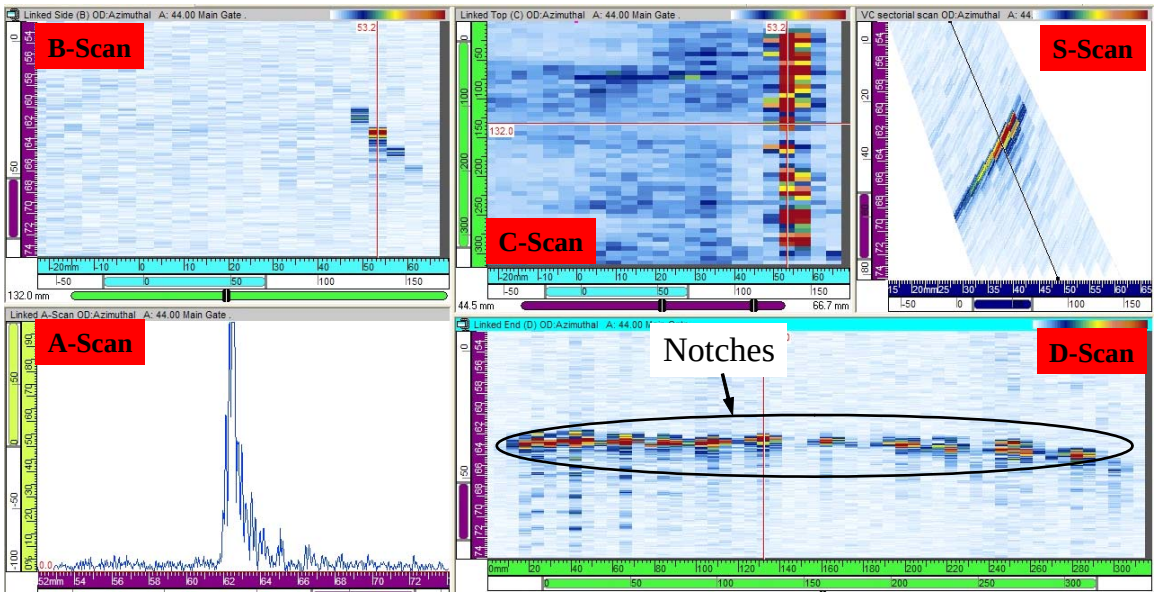


**Figure 1.4.3-9. PA AUT Scan of OD Notches Oriented Perpendicular to the Longitudinal Pipe Axis**

Three girth weld calibration samples, fabricated by three different AUT vendors, were evaluated by EWI. The calibration samples were typical of those used for girth weld inspection in accordance with ASTM E-1961 and were designed for use on 91.4-cm (36-in.)-diameter pipe having a 14.9-mm (0.587-in.) wall thickness. The samples were fabricated for use on a CRC weld bevel having a 5-degree bevel in the fill zones. One calibration sample contained 2-mm (0.08-in.)-diameter FBHs for the weld bevel fusion zones (Fills 1 and 2) and the other two samples had 3-mm (0.12-in.)-diameter FBHs for the weld bevel fusion zones. This provided a good comparison of the sensitivity level differences between 2- and 3-mm diameter FBHs when using the tandem pitch-catch ultrasonic technique.

For the evaluation, two PA tandem techniques were developed. The first technique used a 45-degree transmit beam and a 55-degree receive beam. The 45-degree beam contacted the FBH on the second leg and the 55-degree beam received on the first leg. The second technique also used a 45-degree transmit beam and 55-degree receive beam; however, for the second technique the 45 degree again contacted the FBH on the second leg but the 55-degree beam received on the third leg (Figure 1.4.3-10). Both techniques are commonly used for inspection of the fill zones for this weld bevel and material thickness combination.

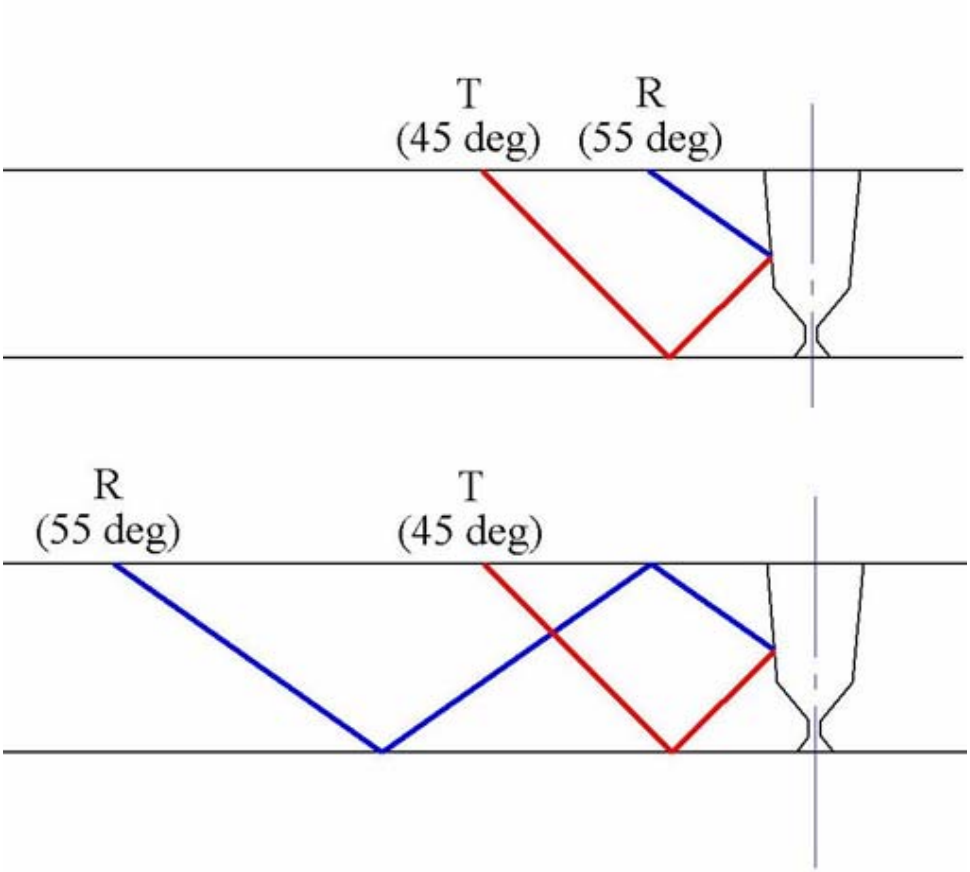


**Figure 1.4.3-10. Tandem Techniques for Detection of Weld Bevel Fusion Flaws**

The two techniques were first tried with a 4-MHz, 64-element, PA probe and then duplicated using a 7.5-MHz, 60-element, PA probe. The results showed similar trends between the two probes with the average sensitivity level from the 2-mm FBH calibration being slightly greater than two times (6.5 dB) that of the 3-mm FBH calibration.

Although FBH reflectors are typically used for tandem pitch-catch calibration, during this project P/E PA data was also collected from the 2- and 3-mm FBHs to obtain an order-of-magnitude comparison of the sensitivity levels. It was found that both the 2- and 3-mm-diameter holes gave similar reflected amplitudes. This can be attributed to the fact that most of the sound energy reflects from the face of the FBH and only the corners of the hole are actually detected (refer to Figure 1.4.3-3). When using the P/E technique, the average signal amplitude from the FBHs in these samples was approximately 21 dB less than the signal amplitude from a 1.2-mm SDH at a depth of 25.4 mm.

Since two girth weld calibration samples had 3-mm FBHs, and were fabricated by different vendors, a comparison was made between the sensitivity levels of the two samples. Using the

4- and 7.5-MHz PA pitch-catch techniques signal amplitudes from the Fills 1 and 2 zones were measured on each sample. The results showed that the average variation in signal amplitude was 1.1 dB for the 4-MHz technique and 1.2 dB for the 7.5-MHz technique. This variation was not considered to be significant and would be consistent with tolerances given in Annex A3 of ASTM E-1961.